J Neurophysiol 104: 811–828, 2010.
First published May 26, 2010; doi:10.1152/jn.01114.2009.

Matching the Oculomotor Drive During Head-Restrained and Head-Unrestrained Gaze Shifts in Monkey

Bernard P. Bechara[1,4] and Neeraj J. Gandhi[1,2,3,4]
[1]*Departments of Bioengineering,* [2]*Otolaryngology and* [3]*Neuroscience,* [4]*Center for Neural Basis of Cognition, University of Pittsburgh, Pittsburgh, Pennsylvania*

Submitted 18 December 2009; accepted in final form 20 May 2010

Bechara BP, Gandhi NJ. Matching the oculomotor drive during head-restrained and head-unrestrained gaze shifts in monkey. *J Neurophysiol* 104: 811–828, 2010. First published May 26, 2010; doi:10.1152/jn.01114.2009. High-frequency burst neurons in the pons provide the eye velocity command (equivalently, the primary oculomotor drive) to the abducens nucleus for generation of the horizontal component of both head-restrained (HR) and head-unrestrained (HU) gaze shifts. We sought to characterize how gaze and its eye-in-head component differ when an "identical" oculomotor drive is used to produce HR and HU movements. To address this objective, the activities of pontine burst neurons were recorded during horizontal HR and HU gaze shifts. The burst profile recorded on each HU trial was compared with the burst waveform of every HR trial obtained for the same neuron. The oculomotor drive was assumed to be comparable for the pair yielding the lowest root-mean-squared error. For matched pairs of HR and HU trials, the peak eye-in-head velocity was substantially smaller in the HU condition, and the reduction was usually greater than the peak head velocity of the HU trial. A time-varying attenuation index, defined as the difference in HR and HU eye velocity waveforms divided by head velocity [$\alpha = (\dot{H}_{hr} - \dot{E}_{hu})/\dot{H}$] was computed. The index was variable at the onset of the gaze shift, but it settled at values several times greater than 1. The index then decreased gradually during the movement and stabilized at 1 around the end of gaze shift. These results imply that substantial attenuation in eye velocity occurs, at least partially, downstream of the burst neurons. We speculate on the potential roles of burst-tonic neurons in the neural integrator and various cell types in the vestibular nuclei in mediating the attenuation in eye velocity in the presence of head movements.

INTRODUCTION

To align the visual axis on an object of interest, one must shift the line of sight (gaze) by rapidly moving the eyes in their orbits. For large changes in gaze, a head movement typically accompanies the eye-in-head rotation. Such rapid, coordinated movements of the eyes in the orbits and the head in space are termed head-unrestrained (HU) gaze shifts. For smaller changes in gaze or when the head is immobilized, redirections of the visual axis are executed by eye movements within the orbits. We refer to such high-velocity movements as head-restrained (HR) gaze shifts or saccades.

The primary oculomotor drive that produces a saccadic rotation of the eyes in orbits is an eye velocity command from neurons in the saccadic burst generator (Robinson 1975). For horizontal eye movements, the eye velocity command is encoded as a high-frequency volley of action potentials by putative short-lead burst neurons (Van Gisbergen et al. 1981) that reside in the paramedian pontine reticular formation (PPRF) and project directly to the abducens motoneurons (Langer et al. 1986; Strassman et al. 1986a). When the head is restrained, properties of the burst specify parameters of the saccade. For example, the number of spikes is linearly correlated with saccade amplitude (Cohen and Henn 1972; Keller 1974; Luschei and Fuchs 1972), and the time varying burst pattern can account for the eye velocity waveform (Van Gisbergen et al. 1981). The same neurons also discharge a high-frequency burst during HU gaze shifts, although the correlation with the eye component is significantly weaker (Ling et al. 1999). However, a degraded association between parameters of the burst and eye-in-head movement does not imply that these burst neurons do not encode the eye-in-head component. The mismatch between the intended and executed eye movement could result from differential contributions from, for example, vestibular and neural integrator inputs to the extraocular motoneurons in the HR and HU conditions (Cullen and Guitton 1997b; Ling et al. 1999; Sparks 1999; Sparks and Gandhi 2003).

We sought to characterize the mismatch between the motor command issued by burst neurons and the executed movement when the head is unrestrained. Thus the primary aim of the present study was to identify how gaze and eye-in-head components differ when an "identical" oculomotor drive—alternatively, the equivalent eye velocity command—from the putative burst neurons is used to produce HR and HU gaze shifts. To address this objective, the activities of individual pontine burst neurons were recorded during HR and HU gaze shifts. Data were collected from both excitatory burst neurons (EBNs) and inhibitory burst neuron (IBNs) and pooled (e.g., Sylvestre and Cullen 2006) into a collective group of burst neurons (BNs). Analogous to template-matching algorithms used in previous studies (e.g., Cullen et al. 2004; Tabak et al. 1996), the burst profile recorded on each HU trial was compared with the burst waveform of every HR trial recorded for the same neuron. The primary oculomotor drive was assumed to be comparable for the pair yielding the lowest root-mean-squared error. Differences in movement properties were then analyzed for each "matched pair." Analyses showed that both eye amplitude and peak eye velocity were significantly reduced in the HU trial of the matched pair, and this effect increased with the amplitude of the HU gaze shift. Furthermore, the reduction in the peak eye velocity was typically several times greater than the head velocity measures associated with the paired HU trial. These results highlight the importance of other inputs (e.g., burst-tonic cells in the prepositus hypoglossi and differ-

Address for reprint requests and other correspondence: R. Gandhi, 203 Lothrop St., Eye and Ear Institute, University of Pittsburgh School of Medicine, Pittsburgh, PA 15213.

ent types of vestibular neurons) onto the extraocular motoneurons in attenuating the eye velocity in the presence of a head movement.

A preliminary version of this study have been published previously (Bechara and Gandhi 2008).

METHODS

Surgical methods

Approval for this study was granted by the Institutional Animal Care and Use Committee for the University of Pittsburgh, and all procedures were in compliance with guidelines of the Public Health Service Policy on Humane Care of Laboratory Animals. Two male rhesus macaque monkeys (*Macaca mulatta*) served as subjects. Under aseptic techniques and isoflurane anesthesia, each monkey underwent surgery to implant a Teflon-coated stainless steel coil beneath the conjunctiva of one eye. In the same procedure, a head restraining post was attached with bone cement (Palacos) to titanium screws implanted in the skull. A second Teflon coated coil was also placed in the bone cement to monitor head position. In a second surgical procedure performed following training on behavioral tasks (see following text), a stainless steel chamber was secured over a craniotomy. The receptacle was tilted 26° in the frontal plane. Microelectrode penetrations from this angle provided access to the excitatory and inhibitory burst neuron regions on both sides of the midline.

Experimental setup and behavioral tasks

Monkeys were trained to sit in a primate chair that was equipped to easily restrain or mobilize the head during HR and HU tasks, respectively. Control of the experimental setup and data collection was accomplished by custom software written using the LabView real-time module (Bryant and Gandhi 2005). Visual targets were presented on a cylindrical board fitted with tri-state light emitting diodes (LEDs) that spanned 96° horizontally and 80° vertically in 2° increments. A miniature laser module was mounted on the head-restraint post. When turned on, the laser emitted a red beam and served to provide visual feedback regarding head position (Gandhi and Sparks 2001). The magnetic field induction technique (CNC Engineering) was used to sense gaze (eye-in-space) and head-in-space positions from the stainless steel coils implanted on the eye and head, respectively. Moreover blinks were recorded by taping a stainless steel coil on the monkey's eye lid during the experiment. Additional details on blink measurements can be found elsewhere (Gandhi and Bonadonna 2005). Gaze, head, and blink position data were sampled at 1 kHz. Eye-in-head (eye) position was calculated on-line as the difference between gaze and head positions. In the HR condition, during which the head was restrained in the straight-ahead position, gaze and eye positions were identical.

When the head was restrained, the monkey was presented with a delayed saccade task. The animal was required to first direct its visual axis on a green LED. While maintaining this fixation, a yellow LED was presented in the periphery. After a random delay period (300-1,000 ms) the green LED was turned off, which cued the monkey to perform a HR gaze shift toward the yellow LED to receive a liquid reward. To achieve a wide range of saccade amplitudes, the position of the green target was either varied or shifted to an eccentric location. As a consequence, the eyes were not always initially centered in their orbits. When the head was unrestrained, the monkey was presented with a delayed gaze shift task associated with a head alignment requirement. In this task, the head-mounted miniature laser and a red LED were illuminated, and the animal had to align both the laser and its gaze with the red stimulus. This step ensured that the eyes were roughly centered in their orbits because both gaze and the head were aligned on the same target. After a random period of gaze and head fixation (400–800 ms), the laser was turned off, and the red LED was switched to green. The animal had to continue to fixate the green LED for another 500–900 ms, but no additional constraint was placed on the head alignment. As the monkey maintained fixation, a yellow LED was presented in the periphery. The animal was required to hold fixation on the green LED for a random delay period (300-1,000 ms), after which the green LED was turned off. The animal then initiated a gaze shift to the yellow LED and held fixation for 500–900 ms to obtain the liquid reward. For both HR and HU tasks, visual fixation and head alignment were required to be within 4 and 7° radius windows, respectively. All target presentations were positioned on the horizontal meridian within ±40° of straight ahead direction. This approach permitted us to gather a database of horizontal movements the amplitude of which spanned the spectrum of amplitudes.

Although we have previously demonstrated the ability to experimentally control the initial eye-in-head position (IEP) in head-unrestrained monkeys (Gandhi and Sparks 2001), there are several reasons why we didn't match the IEPs in HR and HU conditions. Suppose that the IEP was set to zero for both HR and HU conditions. Then the range of HR amplitudes available for our database would be limited to ~30°. This approach wouldn't have produced any good fits for larger amplitude HU gaze shifts. Alternatively, we could have set IEP to an eccentric location contralateral to the direction of the gaze shift. While this configuration would yield a large range of HR amplitudes, comparable amplitude HU gaze shifts, however, would have small amounts of head contributions. This wouldn't be the ideal dataset for our analysis as substantial head movements were necessary during the gaze shifts.

Single unit recordings

Tungsten microelectrodes (~1.5 MΩ impedance, Microprobe) were used to record extracellular activity of burst neurons within the PPRF. Well isolated action potentials were amplified, filtered, detected using a window threshold discriminator, and time-stamped at a frequency of 20 MHz. Spike times were first recorded as the animal performed the oculomotor tasks in one condition (e.g., head-restrained). After a sufficient number of trials was collected, the head was unrestrained (or restrained, if the head was initially free to move), and the activity was recorded as the animal produced movements in the second condition (e.g., head-unrestrained). We judged that isolation was maintained if the spike waveform and signal-to-noise ratio remained comparable (typically 2–4) for the HR and HU conditions. We also took into account similarities in firing patterns (prelude, burst intensity, background activity), as heard on the audio speaker, to assess whether the neuron remained at the electrode tip. In some cases, the electrode was moved a few micrometers to improve isolation.

We focused our efforts on isolating and recording the activities of BNs identified by their locations and discharge characteristics. Excitatory burst neurons (EBNs) are found 1–2 mm rostral to the abducens nucleus and 0.5–1.5 mm from the midline, while inhibitory burst neurons (IBNs) are located 0–2 mm caudal to the abducens nucleus and 0.5–1.5 mm from the midline (e.g., Strassman et al. 1986a,b). Anatomically, the EBNs project to the IBNs and both groups innervate the abducens nucleus (Strassman et al. 1986a,b). Both cell types exhibit similar discharge characteristics during saccades. They emit a high-frequency burst preceded by a negligible or nonexistent prelude and a high correlation between the number of spikes in the burst and HR saccade (Cohen and Henn 1972; Cullen and Guitton 1997a; Kaneko et al. 1981; Keller 1974; Luschei and Fuchs 1972; Scudder et al. 1988; Yoshida et al. 1982) or HU gaze amplitude (Cullen and Guitton 1997b; Ling et al. 1999; Walton and Freedman 2009). These properties have often led to a combined treatment of EBNs and IBNs into one group of burst neurons (e.g., Sylvestre and Cullen 2006). The EBNs and IBNs in our sample also exhibited similar discharge properties, and we have pooled them together as well.

The so-called long-lead burst neurons (LLBNs) can be intermingled with the BNs (Cullen and Guitton 1997a; Keller et al. 2000) and are also located more rostral in the PPRF (Kaneko 2006). They are believed to provide a potent input to the putative BNs but not to the motoneurons directly (see review by Scudder et al. 2002). The LLBNs exhibit a low frequency prelude that precedes the burst, and many are active for only a limited range of saccade amplitudes (Hepp and Henn 1983; Kaneko 2006; Keller et al. 2000). Every neuron in our dataset discharged for all ipsiversive HR and HU movements, and none showed a long lead response prior to the movement. Thus our sample of neurons was most likely void of LLBNs.

While the PPRF is generally believed to control the horizontal component of eye movements, the BNs in this region can discharge for a large range of directions, including purely vertical movements (Van Gisbergen et al. 1981). In fact, the direction for which the neuron fires optimally can often be tilted away from the horizontal axis (Cullen and Guitton 1997a; Quaia and Optican 1997; Scudder et al. 1988; Strassman et al. 1986a,b). We did not attempt to determine the actual preferred direction of an isolated neuron, partly because our analysis is not sensitive to this parameter. We only required that a robust burst be present during horizontal HR and HU movements.

Data analysis

Data were analyzed off-line using Matlab and custom software. For behavioral data, the onset and offset of gaze and eye-in-head components were identified using a velocity threshold criterion of 50 and 30°/s, respectively. Because head movements tend to be longer in duration, slower in both initial and peak velocity, and more variable than gaze shifts, a slightly more complex velocity threshold algorithm was used as described previously (Walton et al. 2007). Briefly, onset and offset were determined when a certain percentage of A/D points within a sliding window, as opposed to all of them, were found to be above (onset) or below (offset) a 6°/s velocity threshold. In our dataset, head movements rarely preceded gaze onset. Thus gaze and eye onsets were identical, and we often refer to them interchangeably.

The likelihood of naturally occurring blinks with gaze shifts increases with HU gaze (or head) amplitude (Evinger et al. 1994). Furthermore, such gaze-evoked blinks alter the dynamics of the eye velocity time profile (Gandhi 2007; Rambold et al. 2002; Rottach et al. 1998). Because we did not want blinks to potentially confound the relationship between BN activity and the observed eye movements, trials in which blinks occurred during gaze shifts were removed from further analyses. Blinks were measured using a velocity threshold (50°/s), and the traces were also inspected visually and corrected to ensure accurate detection.

Burst onset was defined as the instant of the first spike. Burst offset was considered as the time when 95% of the spikes have occurred, a useful criterion for excluding spikes that occur after the end of the gaze shift (Cullen and Guitton 1997a) and often with longer intertrial intervals. Visual inspection was used to verify the automatic detection measures. The spike density function of BNs was obtained by convolving a Gaussian function ($\sigma = 5$ ms) with the spike train. The spike density waveform $FR_{BN}(t)$ recorded during each *HR saccade* was modeled as a function of eye velocity $\dot{E}(t - t_d)$, shifted by a time delay t_d, plus a bias term b: $FR_{BN}(t) = b + r^*\dot{E}(t - t_d)$. The proportionality constant associated with eye velocity is denoted as r (Hz $\cdot$ $^{\circ -1}$ $\cdot$ /s^{-1}). The parameter t_d (ms) represents the time needed for the signal from the neuron to reach the muscles, and the time for the muscle to become activated and generate a movement. A range of t_d values (0–25 ms) were tested, and the delay that minimized the root mean-squared error (rmse) between the simulated and actual firing rates was considered optimal. The parameters of the model, b and r, were estimated using a bootstrapping algorithm. For each neuron, *a*) half of the HR trials were picked randomly; *b*) a linear regression ("regress" command in Matlab) was used to estimate the parameters; and *c*) the other half of the trials were used to test the goodness of fit. This three-step procedure was executed 10,000 times to ensure robust calculation of b and r. The goodness of fit of the model with the optimal t_d was determined by calculating the variance accounted for (VAF) criterion, defined as [var(fit − data)]/[var(data)]. Note that the VAF of a linear model is equivalent to the coefficient of determination (r^2) and to the square of the correlation coefficient.

The interspike intervals of putative BNs are reportedly very similar with minimal variability (Hu et al. 2007). We used this approach to not only verify the previous result (and thus our assessment of BNs) but also to identify spikes that were potentially undetected by the window discriminator. In the early phases of analysis, we performed the template matching algorithm (see following text) with and without manually inserting such "dropped" spikes. Because this operation did not change the outcome of the template matching routine, the analyses included here are without manually inserted spikes.

Template matching and attenuation ratio

For analysis at the individual neuron level, burst activity during each HU gaze shift was compared with the activity of *every* HR gaze shift. Suppose that the dataset contained *mu* HU trials and *nr* HR trials for any one neuron. For each HU trial, we formed *nr* pairs; the bursts were aligned on their onset and subtracted on an ms-by-ms basis for the duration of the HU burst. The pair with the lowest root-mean-squared error (rmse) value was considered a "matched pair." Because this procedure is repeated for every HU trial, we obtained *mu* matched pairs for each neuron. These matches were visually inspected to ensure reasonable matching. Note that any given HR burst can be the best match mate of more than one HU trial.

The burst activity associated with the matched pair fulfills our assumption that the oculomotor drive (eye velocity command) is similar for the accompanying HR and HU gaze shifts. We first compared the burst properties (duration, peak firing rate) of the matched pairs. Next we compared movement characteristics (gaze amplitude, eye-in-head amplitude, their corresponding peak velocity measures, and gaze duration) of the matched HR and HU trials. As shown in Figs. 6–9, we used a moving average to consider the difference in the movement metric between paired HU and HR trials as a function of some parameter, such as HU gaze amplitude (varies across figures). Traditionally, a moving window is applied to all the points that fall within a window that spans a specified range of the independent parameter. We applied a slightly modified algorithm. We applied the moving window across a fixed number of consecutive data points. With this approach, the number of matched pairs in each averaging operation is held constant, but the span of the independent parameter could vary. The two approaches yielded qualitatively similar outcomes (not shown), with our implementation producing a slightly noisier average waveform. For the analyses performed on matched pairs pooled from all neurons, we used a window size of 100 points. When we repeated the moving average analysis on individual neurons, we used a smaller window size (≤40 points) that could vary with the number of matched pairs for the neuron.

Finally, we sought to characterize the time course of changes in eye velocity in the presence of a head movement. We defined an attenuation index (α) as the difference between the matched eye velocities in head-restrained ($\dot{E}_{hr}$) and head-unrestrained ($\dot{E}_{hu}$) conditions divide by the head velocity ($\dot{H}$)

$$\alpha = \frac{\dot{E}_{hr}(t) - \dot{E}_{hu}(t)}{\dot{H}(t)} \qquad (1)$$

According to this equation, $\alpha > 1$ implies that the decrease in HU eye velocity is greater than the velocity of the head movement. The index was calculated from onset of the head movement or the gaze shift, whichever occurred second. Trials without a detected head movement were excluded from the analysis. Note that subtraction of transient and time-varying features of the eye-velocity profiles in the numerator and

division by the relatively sluggish and slower head velocity component in the denominator will inherently introduce high-frequency variability in the attenuation index waveform. Thus interpretation of the eye velocity attenuation index profile should be based on the epoch when the head velocity is not negligible.

The burst matching algorithm was applied to the burst corresponding with the primary movement; bursts associated with corrective movements were not combined with the primary movement in the template matching algorithm. Moreover, several studies have highlighted gaze shifts in which eye velocity exhibits a plateau toward the end of large gaze shifts (see, for example, Fig. 1*A* in Choi and Guitton 2009). Simulations by Galiana and colleagues (1992) suggest that, during the plateau phase, burst neurons continue to discharge albeit with an attenuated firing pattern; to our knowledge, electrophysiological recordings of BNs during such movements do not exist in literature. In our dataset, the end of the eye saccade was typically synchronized with the end of the gaze shift. Thus a specific focus on gaze shifts with plateaus in eye velocity was not pursuable.

RESULTS

Neural activity was recorded from a total of 169 neurons in two animals performing oculomotor tasks. Of these, 107 were classified as BNs based on their discharge characteristics. Activity of 38/107 neurons was collected during head-unrestrained gaze shifts only and of 47/107 cells during head-restrained saccades only. This report focuses on data recorded from 22 burst neurons the isolation of which was maintained in both HR and HU conditions. Data from both excitatory (14) and inhibitory (8) burst neurons, as assessed from their locations relative to the abducens nucleus, are pooled together. The number of HU trials for each neuron ranged from 34 to 293 [115 ± 69 (SD); median: 101], and the number of HR trials ranged from 43 to 256 (130 ± 66; median: 120).

Characterizing BNs

Two different analyses were used to determine whether the neurons in our database display discharge properties associated with EBNs and IBNs. The first evaluates static properties of the burst. The number of spikes and duration of the high-frequency discharge have been repeatedly shown to correlate linearly with HR saccade amplitude and duration, respectively. Figure 1*A* shows the best fit lines for the individual neurons in our sample, and the *inset* plots data from one example cell. The mean ± SD slope across these neurons was 0.99 ± 0.38 spike/° (r^2 = 0.85 ± 0.06). Figure 1*B* illustrates the results of a linear analysis between burst and saccade durations, and the *inset* displays data from an individual neuron. The slope across all neurons was 1.01 ± 0.06 (r^2 = 0.92 ± 0.07).

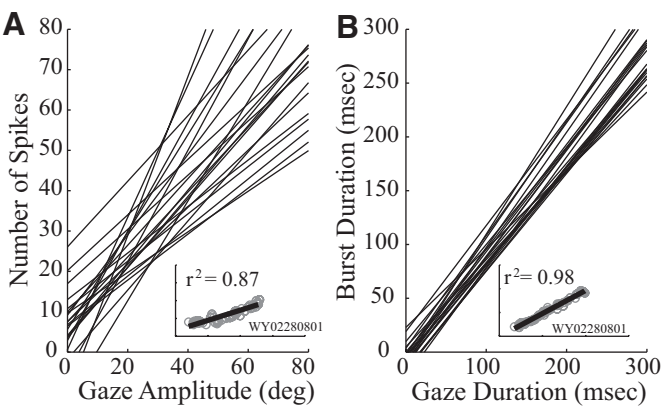

FIG. 1. Correlation between burst and head-restrained (HR) movement metrics. The best linear fit between number of spikes and gaze amplitude (*A*) and burst duration and HR saccade duration (*B*) are plotted. Each line represents a regression fit for 1 cell. *Insets*: data from a representative neuron.

The second analysis relates the temporal features of the neural activity to the accompanying behavioral output. The optimal model (Cullen and Guitton 1997a; Van Gisbergen et al. 1981) describes the burst profile as a function of eye velocity, plus a bias term, when the head is restrained, $FR_{BN}(t) = b + r^*\dot{E}(t - t_d)$. The time-varying functions $FR_{BN}(t)$ and $\dot{E}(t)$ represent firing rate and eye velocity, respectively. The coefficient r indicates the eye velocity sensitivity and has units of spike/°, and the coefficient b represents a constant bias term in units of spikes/s. Also note that $\dot{E}(t)$ is shifted in time by t_d ms to model the neural and mechanical conduction delay between the neuron and the observed movement. The optimal delay t_d was 15 ± 3 ms for the neurons in our study. For this shift, the mean ± SD values for coefficients r and b were 0.69 ± 0.20 spike/° and 142 ± 73 spike/s, respectively (VAF: 0.51 ± 0.14). The collective results of these two analyses are in agreement with previously published reports (Cullen and Guitton 1997a; Van Gisbergen et al. 1981) and, therefore suggest that the data reported in our study are from EBNs and IBNs.

Template matching

For each neuron, the burst profile recorded on each HU trial was compared with the burst recorded for *every* HR movement. The root mean squared error (rmse) of each pair was computed across the duration of the HU burst, and the pair with the minimal rmse was considered the best matched pair. A linear regression was then applied between the HR and the HU bursts for the best pair, and the goodness of the match was assessed in terms of the coefficient of determination (r^2 or VAF). Subplots *A* and *B* of Fig. 2 show the distribution of r^2 as a function of HU gaze amplitude. An ANOVA test yielded a statistically significant effect of gaze amplitude. The data indicate that the r^2 value is high and variability is low for gaze shift up to ~30° in amplitude. For larger movements, the median drops slightly and the variability increases. Across 2,521 trials from 22 cells, the mean ± SD r^2 for the best matched bursts was 0.87 ± 0.13 (median = 0.92; range = 0.013–0.99). For comparison, after randomly pairing a HR burst with each HU burst, the mean ± SD r^2 was 0.34 ± 0.16 (median = 0.37). Figure 2*C* shows the same data in box plot representation but grouped according to the 22 neurons. The median r^2 value was 0.92 across all neurons (range: 0.82–0.97). Additional details on the number of matched pairs for each neuron, as well as statistics on movement amplitudes and the initial eye-in-head positions can be found in Table 1.

Despite the strong correlation between the matched pairs, some trimming was performed. Five percent of the trials with the lowest r^2 values in Fig. 2*A* were omitted to eliminate any outliers. In some cases, the same HR trial was found to be the best match for a large number of HU trials. This was observed across 76 HU trials from two neurons, and we omitted these pairs from our dataset. The mean ± SD r^2 for the remaining 2,318 trials best matched bursts was 0.90 ± 0.08 (median = 0.92; range = 0.63–0.99). The negligible change in the median

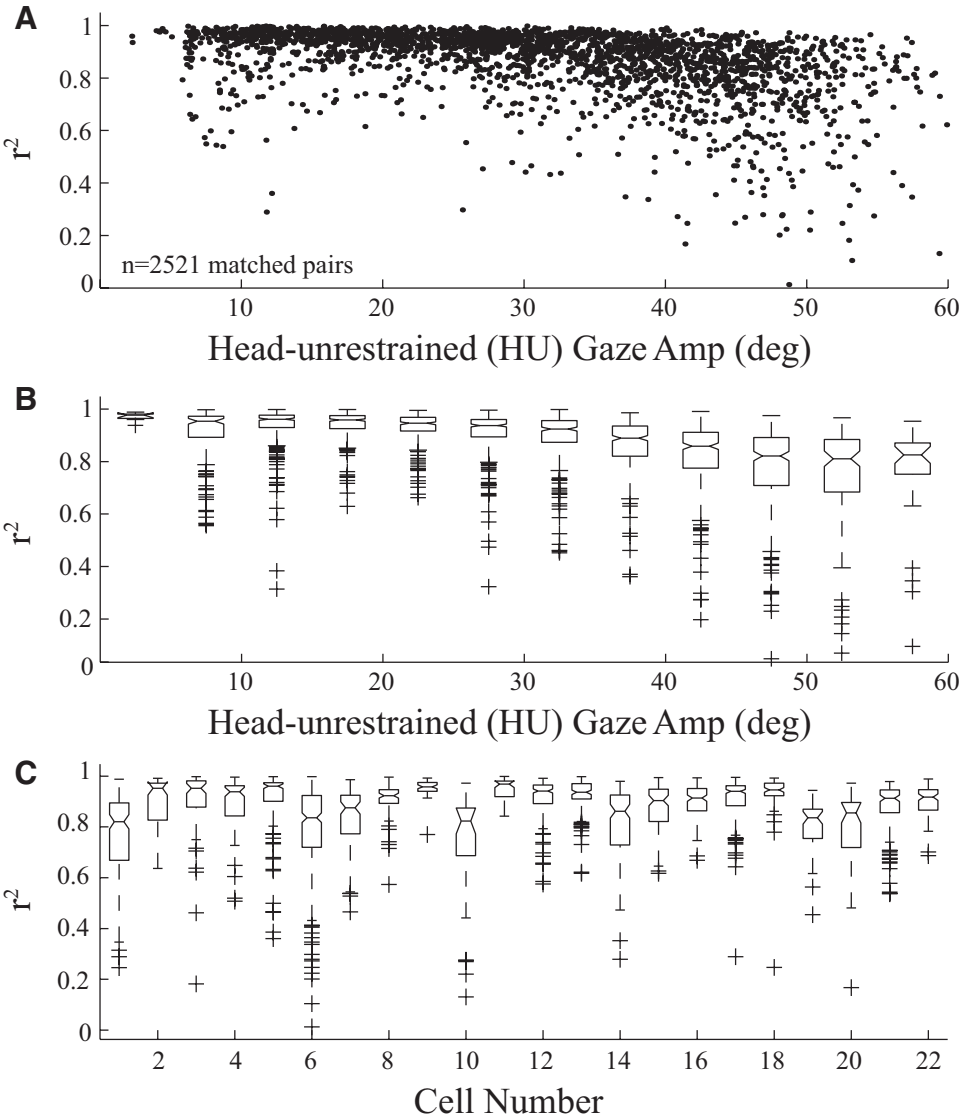

FIG. 2. Distribution of coefficient of determination (r^2). *A*: the r^2 values describing the correlation between the best matched bursts recorded in HR and head-unrestrained (HU) conditions is plotted as a function of HU gaze amplitude. Data are from n = 2521 matched-pairs across 22 burst neurons. *B*: boxplot representation of the same data as a function of HU gaze amplitude. Data are grouped into 5° amplitude bins. On each box, the notched line represents the median, the edges denote the 25th and 75th percentiles. The whiskers span the range of the data not considered outliers, which are plotted individually as crosses. *C*: boxplot representation grouped according to cell number, which also corresponds to the number listed in Table 1.

indicates that the distribution of r^2 values was highly skewed toward larger r^2 values.

Figure 3 displays two examples of best matched bursts and their accompanying eye and head movements, all aligned on eye onset (- - -). The example in the *left column* shows highly correlated HR (blue) and HU (red) bursts (r^2 = 0.91). The HR movement was a 53.2° saccade, and the matched HU gaze shift was 44.6°; its ocular saccade amplitude was 34.8°, and the associated head amplitude was only 10.6°. The *right column* displays another example from a neuron recorded in the other animal (r^2 = 0.93). The HR movement was a 46.6° saccade, and the matched HU gaze shift was 41.5°; its ocular saccade amplitude was 33.3°, and the associated head amplitude was only 13.6°. In both examples, similar burst activity profiles, according to our assumption, serve as the primary eye velocity command (oculomotor drive) to the abducens nucleus. However, the eye-in-head velocity is noticeably attenuated in the HU (red) condition.

This trend was also present for matched pairs with weaker correlations between the bursts. Figure 4 shows two such examples. For the matched pair illustrated in the *left column,* r^2 = 0.66, close to the lower limit of the range included in our analysis. The pair shown in the *right column* has an r^2 value of 0.39. This pair was within the bottom 5% of the r^2 distribution. It was excluded from further analysis, yet it is shown here to provide visualization on the quality of fit of pairs that were omitted. In both examples, the discharge profiles of HU and HR pairs are similar around burst onset, and the early component of the eye velocity (and their peak magnitudes) was significantly lower in the HU trial compared with the paired HR saccade. What can be qualitatively assessed from these examples is that attenuation in eye velocity is substantially greater than the accompanying head velocity.

For the 2,318 matched pairs in our trimmed dataset, we next considered the metrics of the corresponding bursts and movements. Figure 5*A* highlights the linear relationship between the durations of matched HU and HR bursts. The slope was equal to 1.02 (r^2 = 0.90) for data pooled across all neurons. When performing the analysis on individual neurons, the slope was 1.06 ± 0.12 (r^2 = 0.89 ± 0.11). The peak burst frequencies of matched HR and HU trials were also correlated (slope = 0.80,

TABLE 1. *Summary of head-restrained and head-unrestrained movements identified by the burst matching algorithm*

		Head-Restrained (HR) Dataset		Head-Unrestrained (HU) Dataset			
Cell No.	Pairs (n)	Gaze Amplitude,°	Initial Eye Position,°	Gaze Amplitude,°	Head Amplitude,°	Eye Amplitude,°	Initial Eye Position,°
1	159	38.2 ± 7.0 (10.1, 43.5)	−17.8 ± 7.6 (−21.4, −0.1)	40.9 ± 7.5 (6.2, 57.4)	20.7 ± 6.8 (−0.4, 35.9)	20.3 ± 3.7 (6.2, 31.9)	1.9 ± 1.3 (−2.6, 5.2)
2	77	−35.6 ± 14.9 (−55.5, −10.0)	27.6 ± 4.3 (1.3, 28.6)	−32.6 ± 14.3 (−54.5, −8.6)	−13.1 ± 12.6 (−35.6, 0.0)	−19.4 ± 6.9 (−30.1, 9.7)	−1.0 ± 1.2 (−4.1, 1.2)
3	68	−35.1 ± 13.0 (−51.7, −10.1)	20.1 ± 14.4 (−25.9, 29.9)	−32.1 ± 13.8 (−53.0, −6.1)	−13.4 ± 12.7 (−44.2, 0.0)	−18.7 ± 6.4 (−28.7, 8.0)	−1.6 ± 1.3 (−4.5, 1.7)
4	111	31.8 ± 8.9 (6.2, 43.4)	−24.8 ± 0.6 (−26.3, −22.6)	27.1 ± 8.1 (6.0, 41.0)	13.7 ± 12.0 (0.0, 34.7)	13.4 ± 7.2 (−3.5, 25.4)	−0.1 ± 1.3 (−2.2, 3.2)
5	153	−33.4 ± 14.6 (−52.6, −4.2)	27.7 ± 0.9 (25.6, 29.2)	−32.3 ± 13.9 (−56.5, −2.2)	−16.8 ± 13.3 (−49.1, 0.0)	−15.4 ± 6.5 (−27.0, 11.2)	−1.4 ± 1.7 (−12.1, 2.3)
6	293	35.5 ± 19.8 (6.6, 53.2)	−13.4 ± 18.4 (−28.2, 21.3)	34.2 ± 13.4 (6.2, 53.2)	23.4 ± 13.7 (0.0, 47.9)	10.8 ± 7.1 (−24.1, 45.9)	−0.1 ± 2.7 (−8.3, 7.3)
7	99	25.0 ± 13.2 (7.7, 46.8)	−17.5 ± 6.5 (−20.5, 0.2)	25.4 ± 12.5 (6.5, 48.8)	12.5 ± 11.5 (−1.3, 42.7)	12.9 ± 9.4 (−19.3, 47.4)	1.5 ± 4.5 (−6.7, 18.4)
8	76	30.6 ± 14.2 (6.1, 52.3)	−16.1 ± 10.9 (−28.3, 0.4)	29.8 ± 11.5 (8.1, 46.8)	15.9 ± 10.6 (−1.4, 36.6)	13.9 ± 8.5 (−11.6, 31.9)	−0.5 ± 3.5 (−10.6, 10.0)
9	52	23.8 ± 11.9 (8.2, 49.3)	−13.0 ± 15.5 (−27.9, 20.0)	20.2 ± 8.6 (6.1, 37.7)	5.4 ± 7.2 (0.0, 27.0)	14.9 ± 5.0 (6.1, 29.4)	−0.5 ± 2.5 (−5.5, 5.5)
10	34	33.8 ± 9.6 (11.0, 44.0)	−25.3 ± 1.9 (−27.3, −21.4)	38.8 ± 12.1 (5.8, 59.4)	27.1 ± 12.4 (0.0, 45.6)	11.7 ± 12.2 (−22.5, 42.8)	−2.3 ± 5.3 (−10.2, 16.9
11	52	−27.6 ± 17.1 (−54.4, −7.6)	21.7 ± 1.4 (20.9, 25.4)	−21.5 ± 11.9 (−49.9, −7.3)	−12.8 ± 10.9 (−46.6, 0.0)	−8.7 ± 4.2 (−18.3, 4.5)	−1.7 ± 2.3 (−6.9, 2.5)
12	197	32.1 ± 12.9 (7.2, 50.0)	−21.7 ± 0.2 (−22.2, −21.2)	26.7 ± 12.8 (6.0, 52.9)	9.2 ± 10.5 (0.0, 40.8)	17.5 ± 5.3 (−0.1, 26.8)	−1.8 ± 2.3 (−6.5, 8.6)
13	120	−29.7 ± 12.8 (−46.7, −6.1)	20.3 ± 0.5 (20.0, 25.7)	−32.2 ± 15.1 (−59.9, −8.2)	−20.5 ± 14.4 (−51.1, 0.0)	−11.7 ± 5.8 (−50.4, 4.5)	−3.1 ± 3.0 (−11.4, 4.4)
14	129	32.6 ± 13.6 (8.1, 51.8)	−21.2 ± 0.3 (−23.4, −20.6)	29.1 ± 11.4 (11.0, 51.5)	10.4 ± 9.8 (0.0, 35.9)	18.7 ± 5.9 (−8.3, 28.6)	−2.1 ± 2.6 (−7.9, 7.5)
15	94	27.2 ± 8.6 (11.4, 43.5)	−24.1 ± 3.4 (−25.2, −1.1)	24.8 ± 9.1 (8.7, 45.9)	7.4 ± 8.7 (0.0, 41.5)	17.4 ± 6.0 (−8.3, 29.5)	−3.6 ± 2.5 (−9.4, 4.8)
16	131	−38.1 ± 12.9 (−56.1, −7.2)	24.6 ± 0.2 (24.3, 25.3)	−34.1 ± 14.0 (−58.0, −8.3)	−21.0 ± 12.6 (−50.3, 0.0)	−13.1 ± 5.7 (−37.9, 3.2)	−6.3 ± 2.8 (−13.4, 3.7)
17	277	32.2 ± 12.7 (10.6, 56.8)	−23.9 ± 1.0 (−25.5, −19.7)	29.7 ± 12.8 (9.4, 56.4)	11.3 ± 11.3 (−1.2, 44.4)	18.4 ± 6.9 (−16.6, 31.5)	−4.5 ± 3.1 (−12.0, 3.8)
18	67	−36.4 ± 15.2 (−56.3, −9.6)	23.5 ± 0.2 (23.2, 23.9)	−33.0 ± 15.4 (−57.4, −8.7)	−19.7 ± 14.0 (−49.7, 0.0)	−13.3 ± 6.1 (−25.2, 9.1)	−4.9 ± 3.3 (−11.2, 5.1)
19	55	22.3 ± 11.1 (13.1, 49.9)	−23.2 ± 0.5 (−24.1, −22.0)	25.8 ± 10.7 (10.5, 46.9)	8.1 ± 9.3 (−1.6, 36.1)	17.8 ± 9.2 (−9.4, 46.9)	−1.4 ± 4.0 (−12.7, 7.0)
20	49	25.2 ± 16.4 (6.7, 50.3)	−23.8 ± 0.3 (−24.3, −23.0)	29.1 ± 13.0 (6.3, 47.7)	17.1 ± 14.6 (0.0, 48.3)	12.0 ± 10.4 (−27.2, 26.8)	0.0 ± 3.9 (−8.3, 15.1)
21	125	30.7 ± 11.8 (8.7, 55.3)	−23.7 ± 0.8 (−27.6, −22.4)	30.7 ± 12.0 (9.0, 53.9)	18.2 ± 17.4 (−1.2, 66.6)	12.5 ± 13.2 (−27.9, 31.6)	0.8 ± 3.9 (−6.3, 25.6
22	103	27.7 ± 10.9 (11.2, 52.9)	−22.4 ± 0.5 (−23.1, −21.6)	25.6 ± 9.8 (10.0, 47.8)	11.0 ± 13.6 (−0.8, 55.0)	14.6 ± 11.8 (−28.0, 29.7)	−0.9 ± 3.0 (−7.7, 8.2)

Summary data for 22 neurons. The number of matched pairs for each neuron is indicated in the second column. The other columns report mean ± SD values, and the parentheses enclose the minimum and maximum values in the distribution.

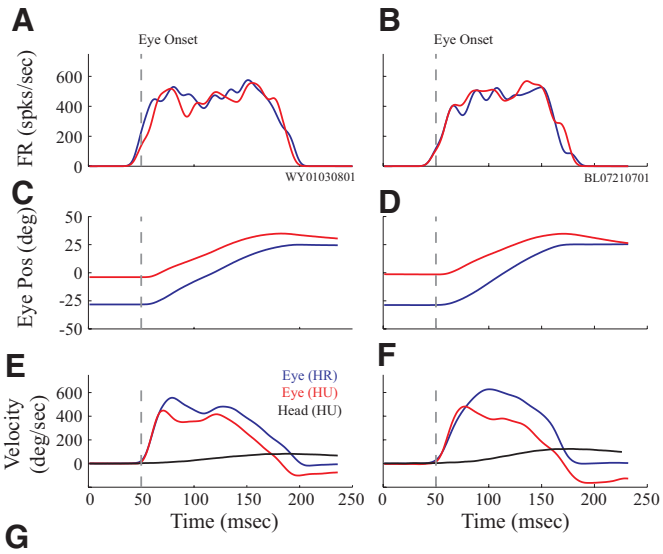

G

Cell Name	r^2 (burst)	HR ΔG=ΔE	HU ΔG	HU ΔE	HU ΔH
WY01030801	0.91	53.2 °	44.6 °	34.8 °	10.6 °
BL07210701	0.93	46.6 °	41.5 °	33.3 °	13.6 °

FIG. 3. Illustration of burst matching algorithm. Two examples of matching bursts (*A* and *B*) and their respective eye position (*C* and *D*) and eye and head velocity waveforms (*E* and *F*). Blue and red traces represent HR and HU trials, respectively. Head velocities for HU condition are shown in black. All traces are aligned on eye saccade onset (- - -). *G*: the table lists the r^2 values characterizing the matched bursts as well as the amplitudes of the gaze shifts and the eye and head components of the paired HU and HR trials.

$r^2 = 0.61$, Fig. 5*C*). When performing the analysis on individual neurons, the slope was 0.69 ± 0.26 ($r^2 = 0.39 \pm 0.20$). Each point in the scatter plots (*A* and *C*) represents one matched pair, and all 2,318 pairs from the 22 neurons are plotted. The large number of points makes it difficult to gauge

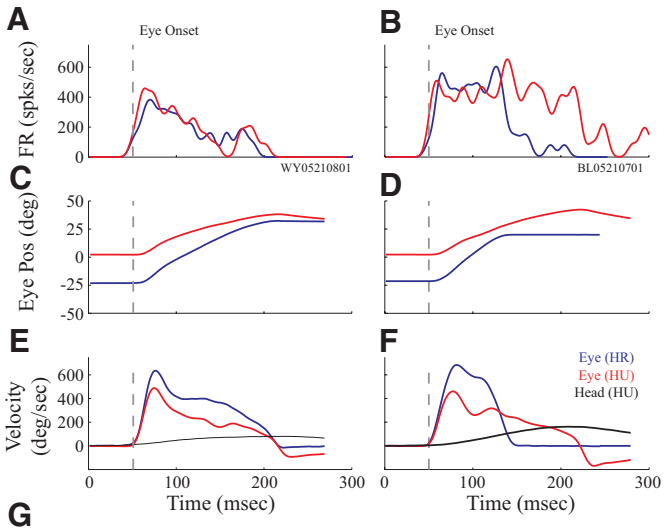

G

Cell Name	r^2 (burst)	HR ΔG=ΔE	HU ΔG	HU ΔE	HU ΔH
WY05210801	0.66	55.3 °	45.6 °	34.5 °	13.6 °
BL07210701	0.39	41.3 °	56.3 °	39.5 °	23.9 °

FIG. 4. Illustration of burst matching algorithm. Same format as Fig. 3, but the 2 examples shown here had lower correlations between the HR and HU bursts of the optimal pair. *Left*: $r^2 = 0.66$ value for the matched pair is toward the lower limit of the range included for further analyses. *Right*: the $r^2 = 0.39$ value for the matched pair is within the lowest 5% of all r^2 values. Hence this pair was not included in further analyses.

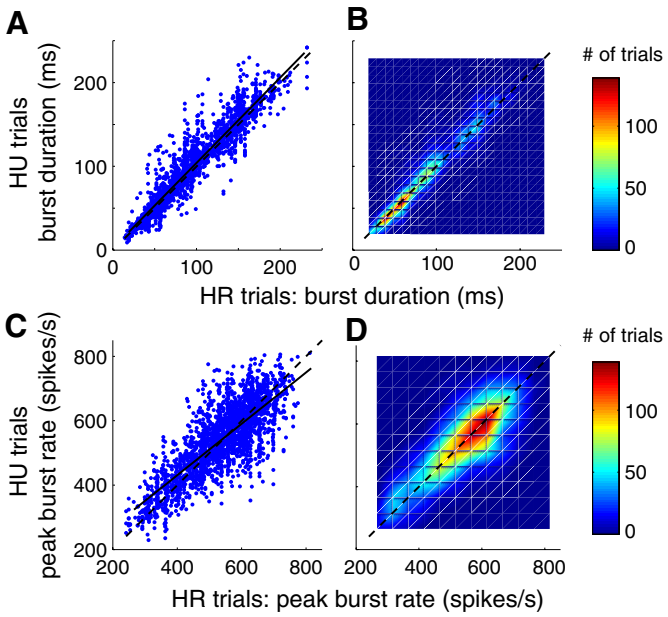

FIG. 5. Comparison of burst metrics of the best match pairs. *A*: burst duration of each HU trial (ordinate) is plotted as a function of its matched HR trial (abscissa). Each symbol represents one matched pair, and data are from all 2,318 matched pairs. —, the best linear fit through the data; slope = 1.02. - - -, unity slope. *B*: visualization of the distribution of data points in *A*. The abscissa and ordinate axes are parsed into 10 ms bins, and the number of trials within each square bin is shown in color according to the axis on the right. The "surf" and "shading interp" commands were used in Matlab to generate this representation. *C* and *D*: analogous figures to compare the peak burst frequency of matched HR and HU trials. Bin width: 50 spike/s.

the distribution of observations. To appreciate the density of points, the same data are plotted as three-dimensional graphs, in which the *z* axis color denotes the number of trials within each square bin (10 ms for *B;* 50 spike/s for *D*). The results of Fig. 5 provide confidence that the template matching algorithm successfully paired HR and HU trials with similar bursts and, presumably, comparable primary eye velocity commands.

For the examples shown in Fig. 3, the eye-in-head saccade amplitude of HU gaze shifts (red) is smaller than the size of its matched HR saccade (blue). This point is further verified by comparing HR gaze amplitude and HU eye amplitude for all matched pairs (Fig. 6*A,* shown in the density distribution format to facilitate visualization). For small HR movements, the matched pairs had similar amplitudes. As HR amplitude increased, which was made possible by varying the initial eye-in-head position, the matching HU eye-in-head saccade amplitude saturated around 25°. A 1-tailed *t*-test verified the visualized result that HU eye amplitude is significantly smaller than the matched HR gaze amplitude. This can also be appreciated in *B,* which plots the difference in eye amplitudes (HU-HR) as a function of HR saccade amplitude. The white and red lines denote the moving average (see METHODS) and 1 SD from the mean, respectively, computed by a sliding window across the 2,318 pairs pooled from all neurons. The same analysis performed individually on each neuron produced a similar finding (Fig. 6*C*). Each color trace illustrates the moving average of one neuron, and the gray shaded area is the range obtained from *B.* The trend of a decreasing difference in eye amplitude (HU-HR condition) with larger movements was present in every neuron, and all but one was within a SD of the moving mean.

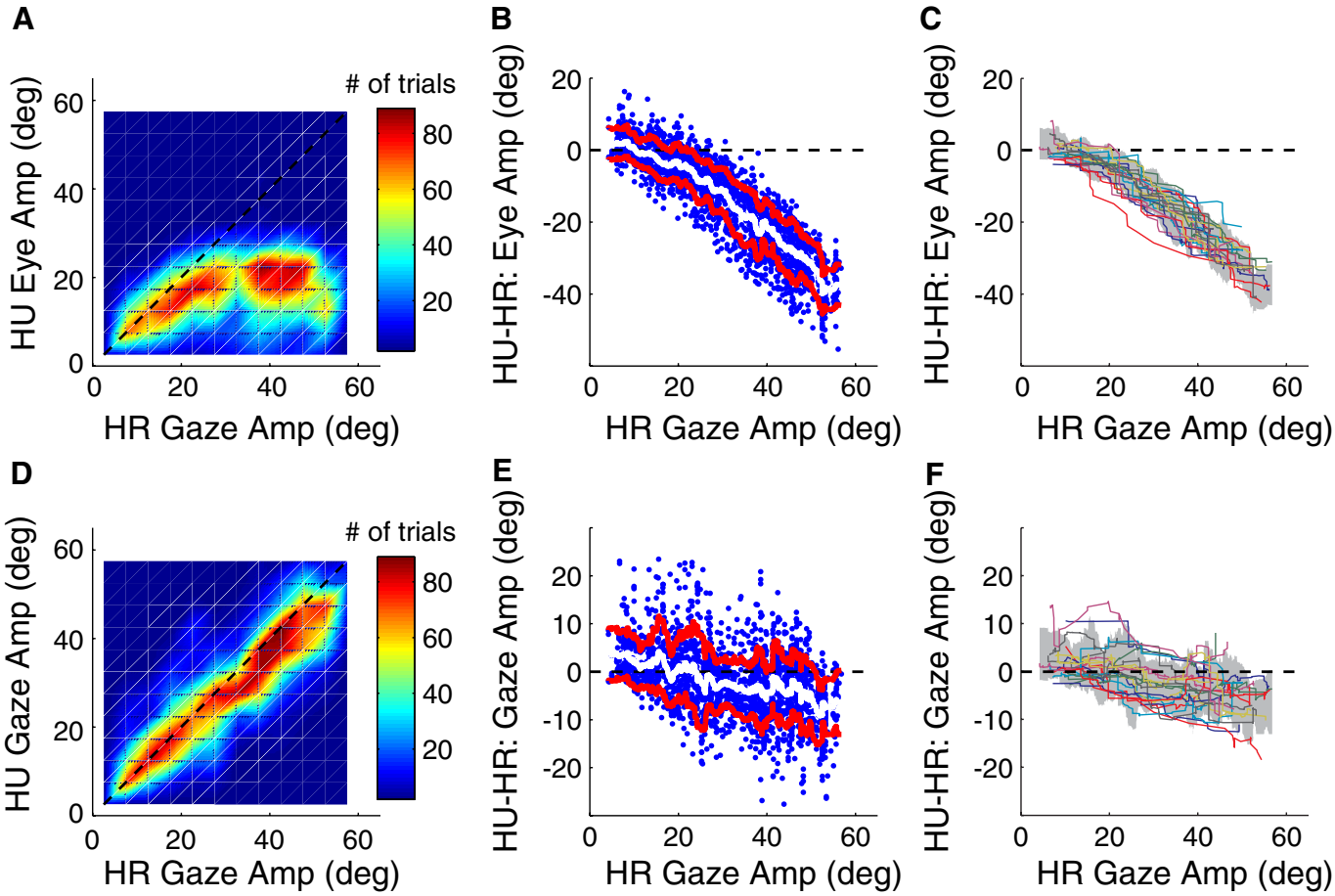

FIG. 6. Comparison of movement amplitude of the best match pairs. *A*: the amplitude of the saccadic eye component of each HU trial is plotted against the gaze amplitude of the matching HR movement. Note that for HR condition, gaze amplitude equals eye saccade amplitude. The color scale indicates the number of trial-pairs in each bin of 5 × 5°. Dashed line, unity slope. *B*: the difference in eye amplitude (HU-HR) is plotted as a function of HR gaze amplitude. White trace, a moving average through the data points; red traces, 1 SD above and below the moving mean. The moving average is computed across all 2,318 trails combined from all neurons. *C*: the moving average analysis is performed separately for each neuron represented as an individual colored trace. The gray shaded area denotes the mean ± SD obtained from *B*. *D–F*: analogous figures to compare gaze amplitudes of matching HU and HR trials. Bin size: 5 × 5°.

We also compared the gaze amplitudes of matched HR and HU movements. Note that for HR trials, gaze amplitude and eye saccade amplitude are identical. The density representation in Fig. 6*D* shows that HR and HU gaze amplitudes increase linearly together with the majority of the points falling along or slightly below the dashed, unity slope line. A linear regression (not shown) yielded a slope of 0.80 (r^2 = 0.74), which was significantly different from one (paired *t*-test, P = 0). Panel *E* plots the difference in gaze amplitude (HU-HR) as a function of HR saccade amplitude. A linear fit (not shown) to the data has a slope of −0.20 and intercept of 4.37 (r^2 = 0.16), and the slope is significantly different from 0 (*t*-test, P = 0). A moving average trace (white curve) also hints that the difference in amplitude becomes larger as HR amplitude increases. However, the zero difference line falls within 1 SD of the mean for nearly the entire span of movement amplitudes. Thus the difference in gaze amplitude of matched oculomotor drive, while statistically different, is small. A similar conclusion is also reached when the moving average analysis is done separately on each individual neuron (Fig. 6*F*).

Figure 3, *E* and *F* also suggest that the peak eye-in-head velocity is lower in the presence of a head movement. Figure 7*A* quantifies this assessment across the distribution of matched pairs. The best fit line (not shown) through the data has slope of 0.37 (r^2 = 0.13), and a paired *t*-test yields a highly significant difference between the two distributions. Panel *B* shows that the reduction in peak eye velocity (HU-HR) increases as a function of HU gaze amplitude, and a linear regression analysis (not shown) demonstrates that the relationship is statistically significant (slope = -6.15 s^{-1}; intercept: 97.80°/s; r^2 = 0.41, P = 0). This trend is present for a pooled population of matched pairs from all neurons (Fig. 7*B*) as well as for matched pairs of nearly every individual neuron (Fig. 7*C*). Thus for the same oculomotor drive, the eyes moved slower in the orbits during a HU gaze shift compared with a HR gaze shift, and this was particularly true for large size movements.

A comparison of gaze velocities of matched pairs suggests that the peak is also reduced for HU movements (Fig. 7*D*). The best fit line (not shown) through the data has slope of 0.40 (r^2 = 0.20), and a paired *t*-test yields a highly significant difference between the two distributions. The reduction in paired, peak gaze velocities as a function of HU gaze amplitude (Fig. 7, *E* and *F*) is not as pronounced as the difference in peak eye-in-head velocity (Fig. 7, *B* and *C*). This can be appreciated by noting that a zero difference in the peak gaze velocities was always within 1 SD of the mean across the entire range of HU gaze amplitude (Fig. 7*E*). The best fit line (not

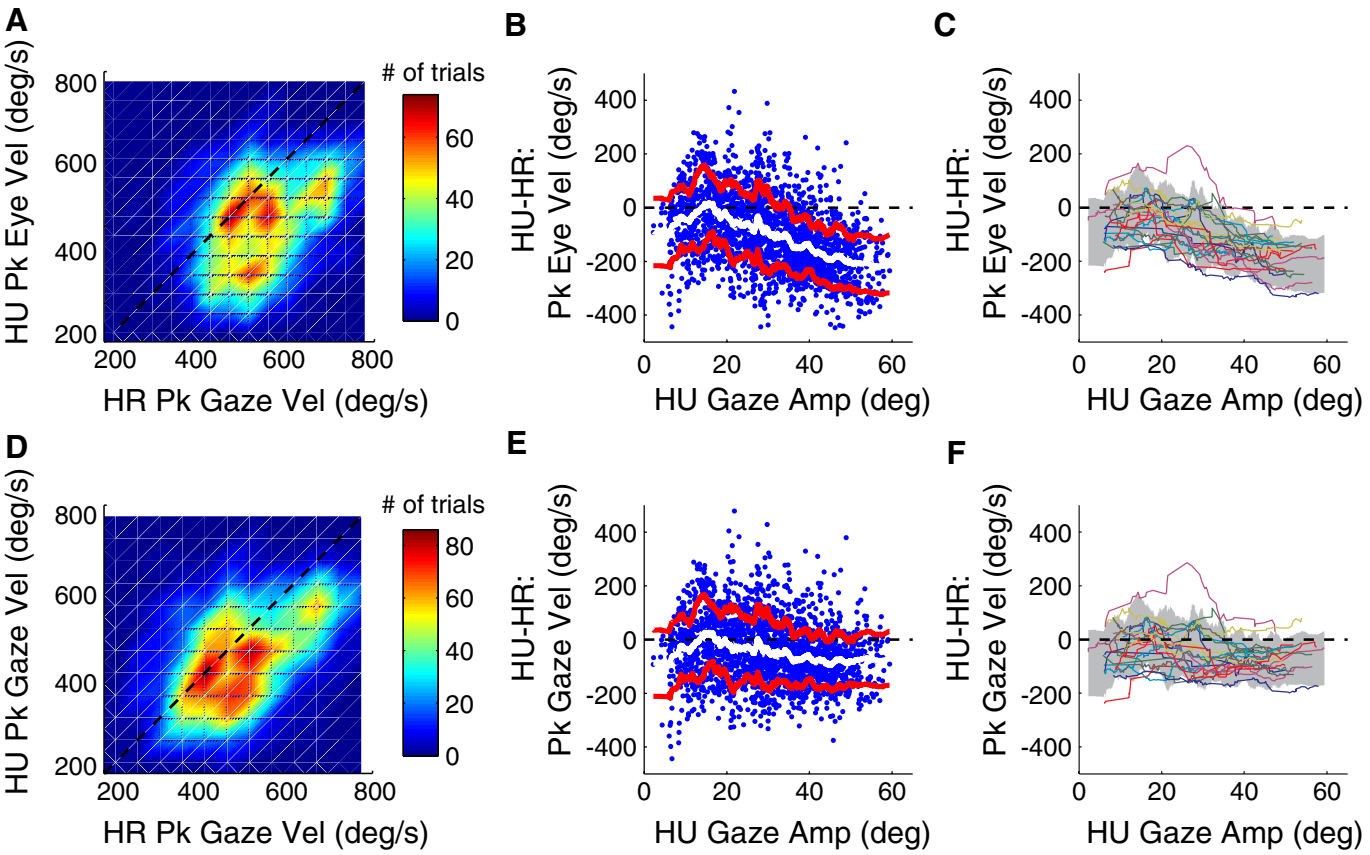

FIG. 7. Comparison of peak velocities of the best match pairs. *A*: the peak eye-in-head velocity of each HU trial is plotted against the peak eye (equivalently, gaze) velocity of the matching HR movement. The color scale indicates the number of trial-pairs in each bin of 50 × 50°/s. Dashed line, unity slope. *B*: the difference in peak eye-in-head velocities (HU-HR) is plotted as a function of HU gaze amplitude. White trace, a moving average through the data points; red traces, 1 SD above and below the moving mean. The moving average is computed across all 2,318 trails combined from all neurons. *C*: the moving average analysis is performed separately for each neuron represented as an individual colored trace. The gray shaded area denotes the mean ±1sd obtained from *B*. *D–F*: analogous figures to compare peak gaze velocities of matching HU and HR trials. Bin size: 50 × 50°/s.

shown) had a much shallower slope (-1.78 s^{-1}), a smaller intercept (6.88°/s), and a weaker correlation ($r^2 = 0.04$) compared with the difference in peak eye velocities.

We also investigated whether the reduction in peak velocity was correlated with properties of the head movement. The difference in peak eye-in-head velocities of matched pairs is plotted as a function of head amplitude (Fig. 8*A*). The parameters of a linear regression fit when head amplitude is the independent variable are as follows: slope = -5.077 s^{-1}, intercept: -22.30°/s; $r^2 = 0.22$. The slope is qualitatively similar to that observed when HU gaze amplitude is the independent variable (Fig. 7*B*). This result is not surprising given that gaze and head amplitudes are correlated for gaze shifts >20° (Freedman and Sparks 1997). The more interesting effect is noted when the difference in peak eye velocities (HU-HR) is plotted as a function of peak head velocity (Fig. 8*B*). The amount of reduction in peak eye velocity in the paired HU trial increases with peak head velocity. The parameters of a linear regression fit are as follows: slope = -1.71 (dimensionless), intercept: -2.95°/s; $r^2 = 0.28$. The yellow line denotes negative unity slope, indicating the region where the reduction in peak HU eye velocity would equal the peak head velocity. Interestingly, however, most of the individual data points (dots) are *below* the yellow line, particularly for HU movements with peak head velocity >50°/s. Thus the magnitude of reduction in peak eye velocity in HU gaze shifts is on average greater than the peak head velocity associated with the gaze shift. Furthermore, note that the time of peak eye velocity, which occurs early in the gaze shift, is typically not synchronized with the time of peak head velocity, which is better time-locked to the end of the gaze shift (see, for example, Fig. 1, *A* and *D* in Chen and Tehovnik 2007); the magnitude of head velocity at the time of peak eye velocity is much lower. Thus for an identical oculomotor drive by BNs in the HR and HU conditions, the reduction in eye velocity during the HU trial is even more exaggerated than that shown in Fig. 8*B*. This point is considered in more detail in the following text, in the section on time varying characteristics of attenuation in eye-in-head velocity.

Figure 8*C* considers the difference in peak gaze velocities of the matched pairs as a function of head amplitude. The parameters of a linear regression fit are as follows: slope = -2.01 s^{-1}, intercept: -12.57°/s; $r^2 = 0.04$. This result parallels the effect noted when HU gaze amplitude was the independent variable: there is a hint of a mild reduction as head amplitude increases, but note that the correlation is very weak. A similar observation emerges when analyzing the differences in peak gaze velocities as a function of peak head velocity (Fig. 8*D*). The parameters of a linear regression fit are as follows: slope = -0.71 (dimensionless), intercept: -2.95°/s; $r^2 = 0.06$. The moving average plot (white traces) roughly parallels the negative unity slope (yellow) line, indicating that the drop in

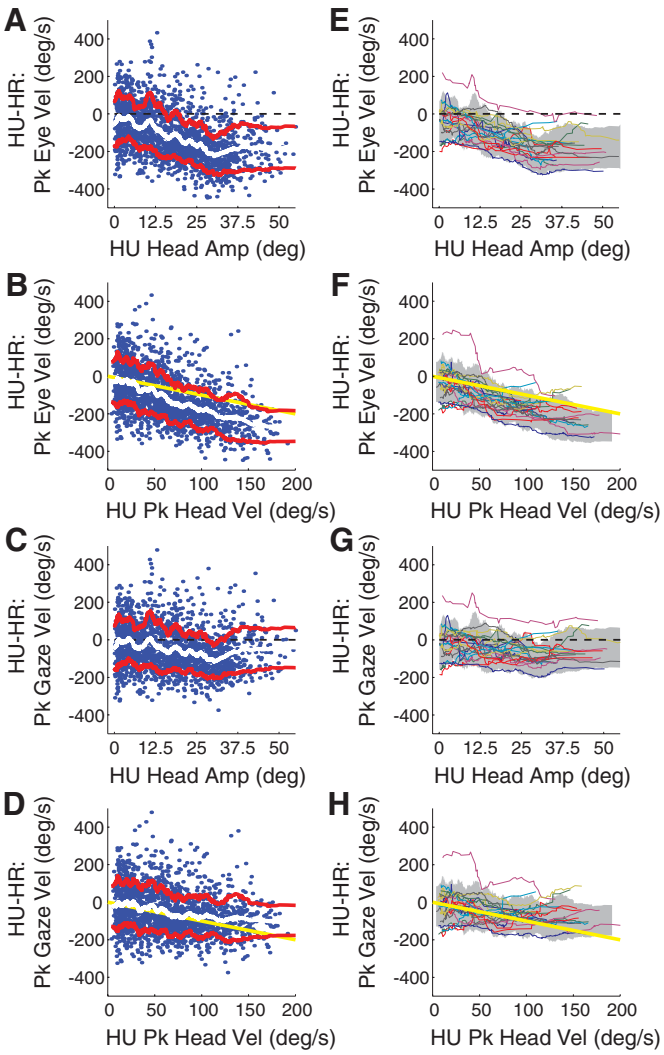

FIG. 8. Differences in peak eye and gaze velocity measures of paired trials as a function of head movement parameters. *A*: difference in peak eye velocity (HU-HR) is plotted as a function of HU head amplitude. *B*: difference in peak eye velocity (HU-HR) is plotted as a function of HU peak head velocity. *C*: difference in peak gaze velocity (HU-HR) is plotted as a function of HU head amplitude. *D*: difference in peak gaze velocity (HU-HR) is plotted as a function of HU peak head velocity. Each dot represents one best matched pair (n = 2,318 pairs). White trace, a moving average through the individual data points; red traces, 1 SD above and below the moving mean; yellow line, a slope of −1. The distribution of individual data points (blue) relative to the yellow line suggests that attenuation in peak eye velocity in HU trial is greater than peak head velocity, particularly for HU trials with peak head velocity >50°/s. - - -, 0 difference in peak velocity. *A–D*: analysis performed across the 2,318 matched pairs pooled from all neurons. *E–H*: same analysis performed separately on each individual neuron, represented as a different colored trace. Gray shaded area, the moving mean ± SD obtained from the corresponding plot (*left*).

peak gaze velocity in HU trials roughly equals the peak head velocity. However, we refrain from any speculation on this observation because the correlation between the reduction in peak gaze velocity and peak head velocity is negligible (r^2 = 0.06).

The analyses reported in Fig. 8, *A–D,* was performed with matched pairs from all 22 neurons pooled together. When the analyses were repeated individually for each neuron, the same general trends were present for each (Fig. 8, *E–H*). In each subplot, each color trace represents one neuron, and the gray shaded region spans one SD from the moving mean (*left*). There is one neuron (magenta trace) that consistently falls outside of the shaded bound region, but even it shows the same general trend as all other neurons. We could not identify anything unusual about this neuron.

Finally, gaze shift durations of matched trials were linearly correlated with a slope of 1.00 and intercept 3.92 (r^2 = 0.85; Fig. 9*A*). The difference in durations of matched HR and HU trials increased slightly with increasing HU gaze amplitude (linear regression result: slope = 0.52 s^{-1}, intercept = −11.46°/s, r^2 = 0.11), although a difference of zero was within one SD across the entire range of amplitudes (Fig. 9*B*). The relationship between the durations of the eye component of matched HR and HU trials was essentially identical (data not shown). The same analysis performed individually on each neuron produced a similar finding (Fig. 9*C*).

Time varying characteristics of attenuation in eye-in-head velocity

INDIVIDUAL TRIAL ANALYSIS. Analyses on kinematic parameters revealed that, for HR and HU trials matched for BN activity, the eye-in-head velocity is attenuated in the paired HU trial (Fig. 7, *A–C*). Furthermore, the decrease in peak eye velocity exceeds the magnitude of peak head velocity (Fig. 8, *B* and *F*). Moreover, because the eye and head velocities peak during different phases of the coordinated eye-head movement, a more appropriate analysis of the attenuation of HU eye-in-head velocity for a matched oculomotor burst should consider the time-varying characteristics of the velocity profiles. For each matched pair, we computed an attenuation index (α) as the difference in HR and HU eye-in-head velocities divided by the corresponding HU head velocity [$\alpha = (\dot{E}_{hr} - \dot{E}_{hu})/\dot{H}$; *Eq. 1*]. Figure 10*A* shows for one matched pair temporal waveforms of HR eye velocity ($\dot{E}_{hr}$, blue), HU eye velocity ($\dot{E}_{hu}$, red) and HU head velocity ($\dot{H}$, black), all aligned on eye onset (vertical gray line) and according to the ordinate scale on the left. The index α (green) resulting from equation 1 is plotted in the same panel with its scale on the right. The two horizontal dotted lines represent α = 0 and α = 1. Near movement onset $\dot{E}_{hr}$ was higher than $\dot{E}_{hu}$, and $\dot{H}$ was relatively small. Consequently, the index started with a large positive value, far greater than one. As the gaze shift progressed, it started to decrease due to an increase in head velocity as well as a decrease in the difference in HR and HU eye velocities. Around and after HU gaze offset, $\dot{E}_{hr}$ becomes zero, and $\alpha = -\dot{E}_{hu}/\dot{H}$. This phase is associated with the eyes counter-rotating in the orbits with a velocity equal and opposite to the head velocity, and the attenuation index α equals ~1.

Just before the end of the gaze shift, the alpha profile often exhibited a transient decrease to negative values. This dip occurs because HR and HU movement durations are slightly different, and therefore the eye velocities reach zero at different time points. For the pair shown in Fig. 10*A,* the offsets were separated by 20 ms (see arrows). The misalignment is due to properties of the template matching algorithm, which did not account for the durations of the bursts or the associated movements. The component of α computed during this mismatch period is shown in magenta.

Figure 10*B* shows α profiles aligned on gaze onset for a family of matched pairs for the same BN (gaze amplitude =

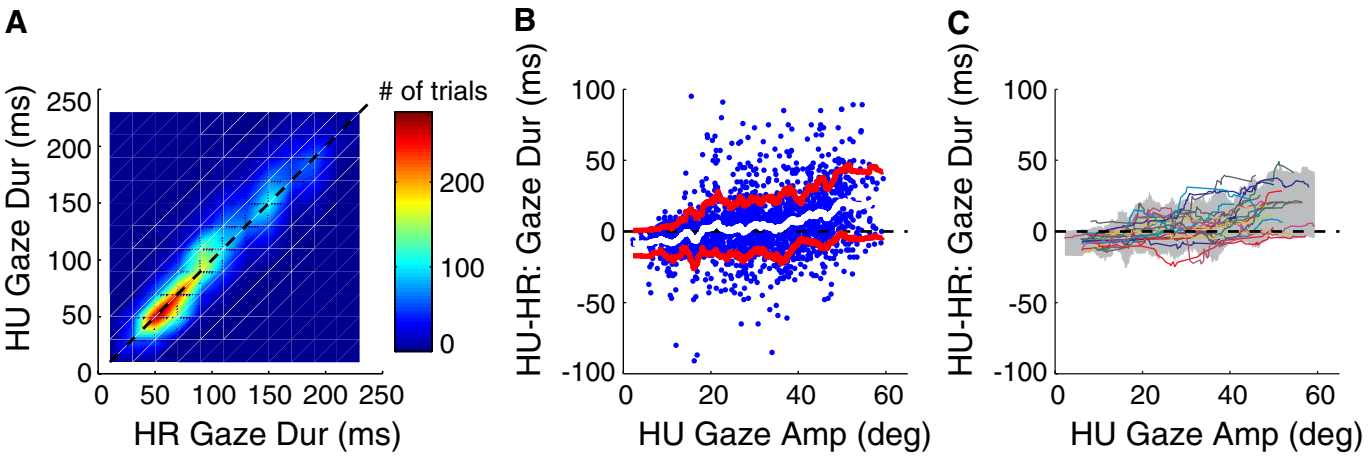

FIG. 9. Comparison of gaze durations of the best match pairs. *A*: gaze duration of each HU trial is plotted against eye duration of the matching HR movement. The color scale indicates the number of trial-pairs in each bin of 20 × 20 ms. - - -, unity slope. *B*: the difference in gaze durations (HU-HR) is plotted as a function of HU gaze amplitude. White trace, a moving average through the data points; red traces, 1 SD above and below the moving mean. The moving average is computed across all 2,318 trails combined from all neurons. *C*: the moving average analysis is performed separately for each neuron represented as an individual colored trace. Gray shaded area, the mean ± SD obtained from *B*.

50.1 ± 0.6°; n = 12). Note that α was highly variable around movement onset; this can be attributed to the fact that the head velocity is relatively low compared with the difference in the eye velocities; dividing by a low number (*Eq. 1*) amplified and exaggerated the minor differences in the initial stages of the eye velocity profiles. However, as the head velocity increased, the α profiles began to merge at a value greater than one. These traces then gradually decreased as in the individual example shown in Fig. 10*A*.

The decreasing trend in attenuation index profiles was prevalent across cells and HU gaze amplitudes. Several examples are illustrated in Fig. 11. Each panel contains six α profiles grouped according to HU gaze amplitude (30 ± 5, 40 ± 5, and 50 ± 5° in the 3 rows) across four representative cells (columns). These profiles are aligned on eye onset. Consistent with the description provided in the preceding text, the α profiles exhibit a highly variable index at the onset of the movement and a transient dip to negative values toward the end of the gaze shift. In between these two epochs, however, the index consistently reaches a value greater than one before decreasing gradually during the gaze shift. At and after gaze shift offset, the index is equal to 1.

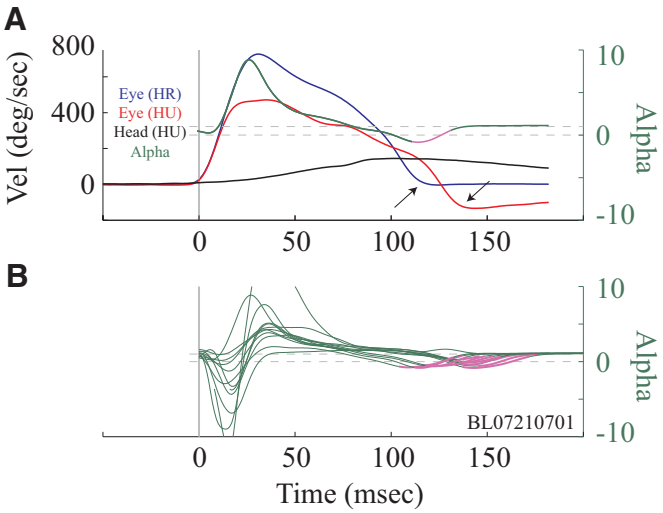

FIG. 10. Temporal features of the attenuation index α. *A*: temporal traces of HR eye velocity (blue), HU eye-in-head velocity (red), and HU head velocity (black) from a best match pair are plotted. *Left*: scale refers to the velocity waveforms. The attenuation index α (green) is computed from *Eq. 1* and corresponds to the scale on the *right*. The offset of the gaze shifts in the HR and HU conditions, as indicated (arrows), are not identical for this matched pair. The component of the attenuation index corresponding to this period is shown in magenta line. The vertical line denotes the onset of the saccadic eye movement. The 2 horizontal dashed lines represent α = 0 and α = 1. *B*: a family of α profiles, each aligned on eye onset, are shown for 50° gaze shifts (n = 12).

Population analysis

Despite the variability in individual α profiles, there is substantial consistency in the waveform across different gaze amplitudes and neurons (Fig. 11). These results suggest that the overlying time course of the attenuation should also be obtainable through a population analysis. All HU trials were sorted according to gaze amplitude and binned in 2° increments. For all neurons, the spike density profiles of all trials within each bin were aligned on burst onset and averaged. The corresponding eye-in-head and head velocity waveforms within each bin were also aligned on gaze onset and averaged. The same procedure was performed on all HR trials. Each averaged HU burst was then compared with the mean HR burst of each bin, and the pair yielding the lowest rmse was considered optimal. Suppose that the HU data were grouped into M bins and the HR date into N bins. The template matching algorithm produced M optimal pairs. The r^2 values across all matched pairs were high across all amplitudes (0.963 ± 0.033; median: 0.974; range: 0.855–0.995). The attenuation index profiles were then computed using *Eq. 1*.

Figure 12 plots the results of the template matching algorithm and the associated attenuation index profiles for 30, 40, and 50° gaze shifts. The average burst profiles show a good correspondence between the average HR (blue) and HU (red) trials; the r^2 values were 0.99, 0.97, and 0.95, respectively. The *middle column* plots the matching eye-in-head velocity profiles. In all cases, the peak eye-in-head velocity is greater for the HR condition. This is clearly represented in the α profiles (*right*). The attenuation index rises quickly to >5 immediately after gaze onset, and it gradually returns to one as the gaze shift

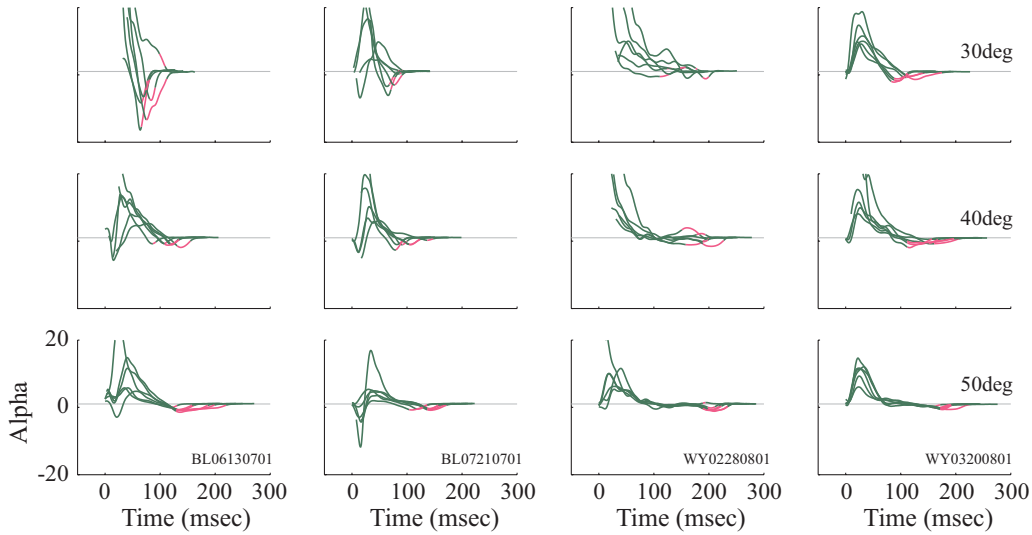

FIG. 11. Family of α profiles across individual neurons and gaze amplitudes. Attenuation index profiles aligned on eye onset and grouped according to HU gaze amplitude (30, 40, and 50°) for 4 example cells. Each panel contains 6 profiles. Dashed horizontal line, $\alpha = 1$.

is completed. This result indicates that for the burst activity across the population of BNs, the reduction in eye velocity (HR-HU conditions) is multiple times the head velocity during the early phase of the gaze shift.

Additional considerations

The preceding analyses ignore two factors that could potentially confound interpretations of the data. The first is that the IEP varied between HR trials but was close to zero for all HU trials. Thus it was important to determine whether matched BN inputs produced eye velocity waveforms that varied with IEP. Previous studies have reported no IEP effects for EBNs (Keller 1974), and a modest effect for some IBNs (Scudder et al. 1988). We acknowledge that our experimental and behavioral designs prevented a direct control of IEP (see METHODS), yet we were able to perform analyses to sense whether this parameter was a major contributor. To address this issue, HR trials for each neuron were grouped by gaze amplitude. The BN activity of each trial was then template-matched with another trial

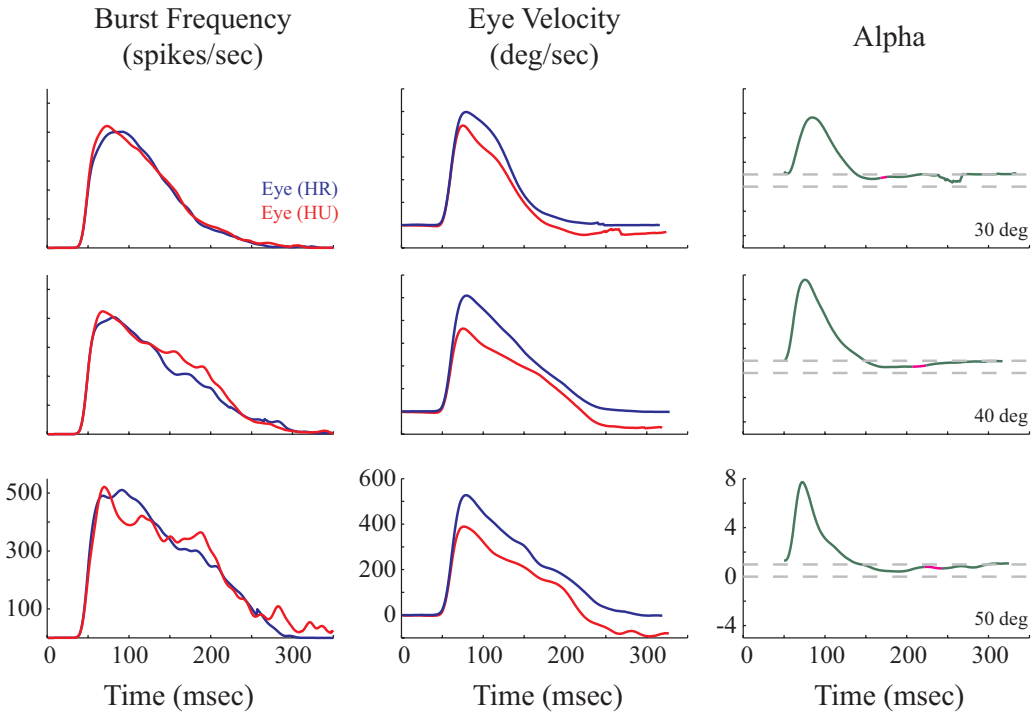

FIG. 12. Template matching and computation of attenuation index at the population response level. *Left*: averaged burst profiles for 30° (*top*), 40° (*middle*), and 50° (*bottom*) HU gaze shifts are shown in red. The best matching averaged burst profile for HR movements is shown in blue. The corresponding, averaged eye-in-head velocity waveforms for the matching HU (red) and HR (blue) conditions are illustrated in the *middle column.* The attenuation index waveforms computed from these eye-in-head velocity traces and corresponding head velocity waveforms (not shown) are shown in the *right panel.* Dashed horizontal lines, $\alpha = 0$ and 1. Note that α profiles are qualitatively similar to the waveforms observed by matching individual trials (Figs. 10 and 11) but with substantially less variability.

within the same group (so that each matched pair of trials had the same gaze amplitude) but with the added constraint that the IEPs be different. Figure 13 shows two examples of best-matched bursts and velocity profiles for HR saccades of 26° (IEP: −26° and 0) and 41° (IEP: −24 and −20°); in the latter case, the large saccade size limited the difference in IEPs that we were able to test. The results show that matched HR trials had similar velocity time profiles and peak velocities. Consistent effects were noted for the four neurons to which this analysis was applied. Linear regression performed between the velocity profiles of all matched pairs activity yielded a slope of 0.98 ± 0.19 and r^2 of 0.97 ± 0.09.

Table 2 provides results of another analysis that evaluated for potential contributions of IEP. In Figs. 6–9, we considered whether a difference in movement parameters (HU-HR) for matched pairs varied with gaze amplitude, head amplitude, or peak head velocity. We applied a linear regression analysis on these parameters and noted the goodness of fit (see r^2 values in *column 4* of Table 2). Next we considered whether the addition of another parameter—the difference in IEP for the matched HU and HR trials—improved the goodness of fit (*column 6*). For regression analyses performed across data pooled from all neurons, incorporating the IEP component produced improved the fit by <3% (*column 7*). When considering the analysis separately for each neuron, some fits were improved by at most ~7%. In both cases, the IEP contribution was small. We took these two results to indicate that there was no significant difference in the profiles of these matched trials.

The second concern involved the timing of the head movement relative to the eye movement and its effect on α. On one hand, the eye movement could be modulated by vestibular signals generated by the head movement. On the other hand, efference copy signals of the impending, active head movement could influence the eye movement ahead of the head movement itself. Therefore it is worthwhile to consider how the attenuation index is altered when eye velocity not only lags but also leads the head movement. For each matched pair, we recomputed all α profiles by shifting head velocity relative to eye velocity in increments of 1 ms, up to ±25 ms. Figure 14 shows the family of α profiles for the same matched pair exhibited in Fig. 3, *B–F*. This approach resulted in increasing the variability of the index, but the overall profile of α remained consistent. Similar families of curves were noted for other matched pairs across different neurons and range of gaze amplitudes. Hence not incorporating the neural transduction time from the vestibular periphery to the extraocular motoneurons does not profoundly change the outcome of our analyses.

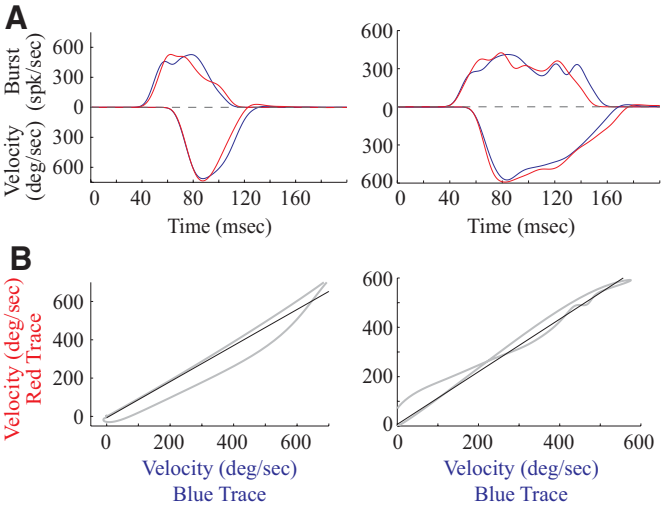

FIG. 13. Lack of effect of initial eye position (IEP) on oculomotor drive of matched head-restrained saccade trials. *A*: burst discharge (*upward plot*) and corresponding, inverted eye velocity profiles (*bottom plot*) of 2 matched pairs from the same neuron. *Left*: saccade amplitude is 26° to the right for both trials with IEP equal to −26° (red) and 0° (blue). *Right*: saccade amplitude is 41° to the right for both trials with IEP set to −24° (red) and −20° (blue). *B*: when the 2 eye velocity profiles are plotted against each other, the trace stays close to the unity slope line (solid diagonal line).

DISCUSSION

Excitatory and inhibitory burst neurons of the PPRF form the major oculomotor input to the abducens motoneurons (Langer et al. 1986) for generation of head-restrained and -unrestrained gaze shifts in the horizontal dimension. We refer to the high-frequency burst associated with these neurons as the oculomotor (or eye velocity) command to the extraocular motoneurons. We matched the high-frequency burst profiles of each BN recorded during both HR and HU gaze shifts and then examined characteristics of eye-head coordination when an "identical" oculomotor command is delivered to the abducens motoneurons in the two conditions. Our results indicate that the amplitude and peak velocity of the saccadic eye component are smaller when the same oculomotor drive is associated with a coordinated eye-head movement as opposed to a head-restrained saccade. At face value, this is not surprising because the vestibuloocular reflex (VOR) is expected to reduce the amplitude and velocity of the eye-in-head component of the HU gaze shift. Attenuation based on a VOR mechanism, however, would be less than or equal to the kinematics of the head movement. What is remarkable about our results, therefore is that the decrease in peak eye velocity is several times *greater* than the increase in head velocity. This observation emerges from both the kinematics analyses as well as the attenuation index that takes into account temporal features.

The impact of these results depends critically on two key assumptions of the study. One, high-frequency burst neurons in the PPRF provide the primary oculomotor input to the abducens motoneurons for the control of horizontal eye movements and, two, matching the bursts during HU and HR gaze shifts means that the oculomotor drive is comparable for the paired movements. We now provide arguments in support of these claims. We also evaluate the implications and sensitivity of the burst matching technique. Finally, we consider the neural elements that most likely account for the enhanced reduction in eye velocity.

Assumptions about the oculomotor input

Nearly all models of the saccadic system use a brain stem burst generator "module" that provides an eye velocity command to the extraocular motoneurons (e.g., Robinson 1975). For horizontal saccades, this function is attributed to the EBNs that project directly to the abducens nucleus (Langer et al. 1986; Strassman et al. 1986a,b). We have also included inhibitory burst neurons, which are driven by and exhibit discharge characteristics similar to the EBNs (Strassman et al. 1986a,b). Both emit a high-frequency burst just before the onset of a saccadic eye-in-head movement. Each discharges for ipsiver-

TABLE 2. *Summary of variance-accounted for (r^2) by linear regression analyses*

Dependent Variable	Database	Independent Variable	R^2	Independent Variables	R^2	ΔR^2
HU-HR: eye amplitude (Fig. 6, *B* and *C*)	22 neurons	HR gaze amplitude	0.77 ± 0.11	HR gaze amplitude, ΔIEP	0.80 ± 0.10	0.027 ± 0.026
	1 "neuron"		0.79		0.80	0.0015
HU-HR: gaze amplitude (Fig. 6, *E* and *F*)	22 neurons	HR gaze amplitude	0.19 ± 0.18	HR gaze amplitude, ΔIEP	0.24 ± 0.18	0.052 ± 0.058
	1 "neuron"		0.16		0.17	0.0064
HU-HR: Peak eye velocity (Fig. 7, *B* and *C*)	22 neurons	HU gaze amplitude	0.21 ± 0.17	HU gaze amplitude, ΔIEP	0.28 ± 0.18	0.067 ± 0.095
	1 "neuron"		0.22		0.24	0.022
HU-HR: peak gaze velocity (Fig. 7, *E* and *F*)	22 neurons	HU gaze amplitude	0.089 ± 0.087	HU gaze amplitude, ΔIEP	0.16 ± 0.16	0.070 ± 0.11
	1 "neuron"		0.049		0.06	0.014
HU-HR: peak eye velocity (Fig. 8, *A* and *E*)	22 neurons	HU head amplitude	0.23 ± 0.14	HU head amplitude, ΔIEP	0.29 ± 0.18	0.065 ± 0.12
	1 "neuron"		0.23		0.25	0.027
HU-HR: peak eye velocity (Fig. 8, *B* and *F*)	22 neurons	HU peak head velocity	0.25 ± 0.15	HU peak head velocity, ΔIEP	0.32 ± 0.18	0.069 ± 0.13
	1 "neuron"		0.29		0.30	0.0080
HU-HR: peak gaze velocity (Fig. 8, *C* and *G*)	22 neurons	HU head amplitude	0.078 ± 0.095	HU head amplitude, ΔIEP	0.15 ± 0.19	0.073 ± 0.12
	1 "neuron"		0.052		0.072	0.019
HU-HR: peak gaze velocity (Fig. 8, *D* and *H*)	22 neurons	HU peak head velocity	0.078 ± 0.082	HU peak head velocity, ΔIEP	0.16 ± 0.18	0.078 ± 0.13
	1 "neuron"		0.071		0.082	0.011
HU-HR: peak gaze Duration (Fig. 9, *B* and *C*)	22 neurons	HU gaze amplitude	0.18 ± 0.18	HU gaze amplitude, ΔIEP	0.21 ± 0.18	0.024 ± 0.037
	1 "neuron"		0.14		0.15	0.0076

ΔIEP, difference in IEP between HU and HR matched pair. Column 4 lists the R^2 value for a linear regression analysis between the independent parameter listed in column 3 and the dependent variable in column 1. Column 6 lists the R^2 values obtained when performing a multilinear regression analysis with one additional parameter (column 5). Column 7 shows the negligible improvement in R^2 by incorporating ΔIEP in the regression analysis. Two rows of data are listed for each dependent variable (associated with a specific figure). The top row lists the results of (multi)linear regression analyses performed separated on each neuron; the R^2 values indicate means ± SD. The bottom row indicates the results when all 2,318 matched pairs across all neurons were pooled together. IEP, initial eye-in-head position.

sive saccades of all amplitudes and, the number of spikes in the high-frequency burst is linearly correlated with the size of HR saccade (Cohen and Henn 1972; Cullen and Guitton 1997a; Kaneko et al. 1981; Keller 1974; Luschei and Fuchs 1972; Scudder et al. 1988; Yoshida et al. 1982). In addition, the burst profile is well described by the eye velocity waveform when the head is restrained (Cullen and Guitton 1997a; Van Gisbergen et al. 1981). The discharge properties of the neurons included in this study conformed to the neural activity of putative EBNs and IBNs. Thus we believe our investigation taps into the primary oculomotor drive to the abducens nucleus. The so-called long-lead burst neurons that are intermingled with EBNs and IBNs were not included in our investigation.

In contrast to results obtained from head-restrained studies, interpretations of the discharge characteristics associated with head-unrestrained gaze shifts have generated substantial debate. Some studies have argued that brain stem burst generator encodes movement commands for the eyes within the orbits (e.g., Freedman 2001). Others have proposed that the output of these neurons better encodes gaze (e.g., Galiana and Guitton 1992). Implicit in the latter statement is that burst neurons send signals to both extraocular and, directly or indirectly, to neck motoneurons (Grantyn et al. 1987). It has also been suggested, however, that the activity of burst neurons encodes temporal features of both eye and head movements but that the neurons project only to the extraocular motoneurons (Cullen and Guitton 1997b). This conceptualization requires that the head movement related signal be subtracted out at the level of the extraocular motoneurons. The strength of our study is that the results are not dependent on knowledge of which and how many effectors, in addition to the extraocular muscles, are influenced by the BN activity. For all intents and purposes, they can project to the neck motoneurons. They can also relay signals, for example, to trunk muscles for coordinated eye-head-body movements or to shoulder muscles for coordinated eye-hand movements. It also doesn't matter whether the neurons encode monocular or binocular movements (Zhou and King 1998) or in fronto-parallel or all three dimensions (Van Horn et al. 2008). The only requirement is that the putative burst neurons project at least to the abducens motoneurons and discharge for every movement that includes a horizontal ocular saccade component.

We thus reasoned that if these BNs relayed the same motor command to the abducens during HR saccades and HU gaze shifts, then the primary oculomotor drive (eye velocity input) is basically identical for the two conditions. The template matching algorithm identified the optimal pair for HR and HU gaze shifts based on a minimum root-mean-squared difference criterion and provided a means to compare characteristics of the paired movements. This approach revealed that the eye velocity is substantially reduced in the HU condition, and, moreover, the attenuation (HR-HU for matched pair) was greater than the head velocity for much of the duration of the gaze shift.

The template matching routine, particularly in its application to compute the attenuation index (*Eq. 1*; Figs. 10–12 and 14), is not without limitations, however. For example, subtraction of transient and time-varying features of the eye-velocity

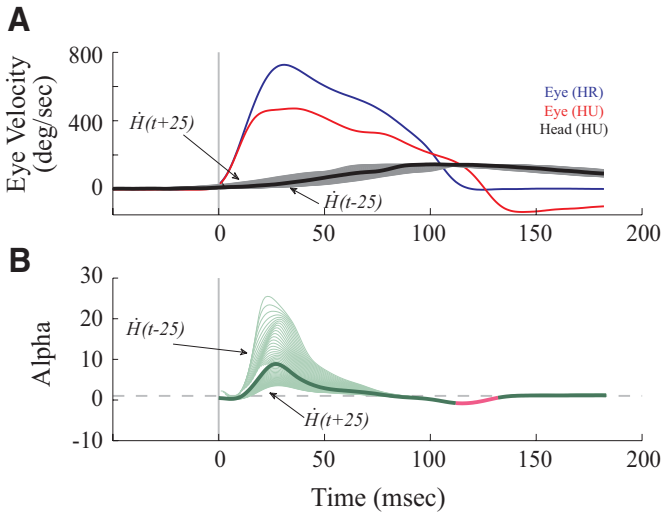

FIG. 14. Effects of shifting the head velocity trace on attenuation index. *A*: temporal profiles of HR eye velocity (blue) and HU eye velocity (red) are shown for 1 matched pair. The black trace represents head velocity (HU trial) with 0 shift. The shaded region encompasses the space spanned by shifting it by ±25 ms in increments of 1 ms. *B*: each thin trace is a profile of index α for each of the head velocity traces. Solid curve, 0 shift in head velocity. The onset of each trace occurs at head or gaze onset, whichever occurs later. Note that the key point of the panel, that the index is high during the gaze shift and gradually approaches 1 as the gaze shift reaches completion, is consistent across all shifts in head velocity. Dashed horizontal line, an index value equal to 1.

profiles in the numerator, combined with division by the relatively sluggish head velocity component in the denominator, will inherently introduce high-frequency variability in the attenuation index waveform. Also the algorithm compares the discharge profiles across the duration of the HU burst. Our implementation did not require that the durations of the HR and HU bursts be identical. Similarly, the durations of the velocity profiles associated with the matched bursts need not be equal. As documented in RESULTS, the mismatch in duration can introduce misleading features to the attenuation index profile, particularly toward the end of the gaze shift.

Although not presented in this manuscript, some of the limitations associated with template matching algorithm were addressed in numerous ways. For example, the duration of the HR velocity waveform was either stretched or interpolated to equate the duration of its paired HU trial; typically, the HR trial was stretched. Conceptually comparable duration normalization routines have been used in previous studies of motor control (e.g., Bock 1990; Lehnen et al. 2009). This procedure successfully removed the transient dip to negative α values toward the end of the gaze shift. One consequence of this technique, however, is that it shifted the alignment of the acceleration phases of HR and HU eye velocities, which produced even more variability in attenuation index at gaze onset. We also tried to apply the burst matching algorithm on three separate, equal duration "chunks" of the eye velocity waveforms. The negative dip at the end of the movement persisted as long as the durations of the last chunk remained mismatched. We also found no appreciable improvements in the early phases of the index profiles. Given the lack of improvement, the reviewers suggested that we exclude additional analyses associated with the attenuation index, and we agreed.

Of course, more than one BN contributes to the generation of an eye-in-head saccade. It is reasonable to argue that matching the burst of one neuron does not imply that the population response is equal for the HR and HU movements. We addressed this concern indirectly by averaging appropriate bursts across all neurons in our database, thereby producing a population response. The template matching algorithm produced the same enhanced attenuation index result (Fig. 12). It also overcame the high variability associated with computing the index for individual matched trials.

A reader still not satisfied about our approach should also consider that a similar interpretation can be reached from at least two different analyses not relying on a template matching algorithm. One, Freedman and Sparks (2000) analyzed changes in eye and head velocities *within* individual gaze shifts and

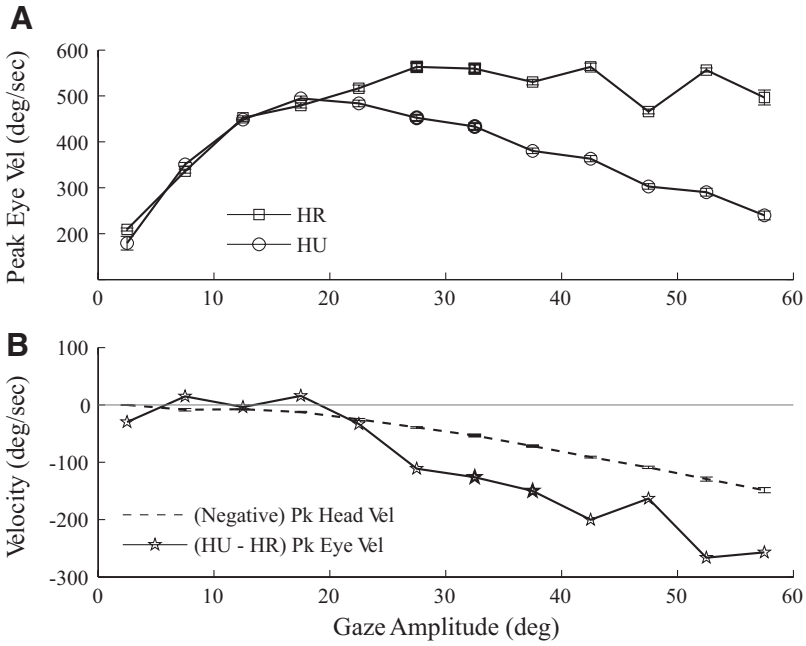

FIG. 15. Main sequence analysis for gaze *amplitude-matched* movements. Note that the data shown in this figure were not subjected to template matching of the burst profiles. *A*: mean peak eye-in-head velocity is plotted as a function of gaze amplitude. Data are binned into 5° increments according to gaze amplitude. HR and HU data are shown in squares and circles, respectively. Error bars mark SEs. *B*: the difference in peak eye velocities (HU − HR) is plotted as a function of gaze amplitude and shown as stars. Negative values on the ordinate scale indicate that for movements grouped according to gaze amplitude (within individual bins), the HU peak eye velocity is less than HR peak velocity. Dashed black trace, the negative of peak head velocity as a function of gaze amplitude (HU condition only). Dashed, horizontal gray line, 0 velocity. Thus for amplitude-matched movements, the reduction in peak eye velocity is greater than the peak head velocity (which occurs later in time). Note that this figure is very similar to Fig. 7*B*, which shows a similar relationship for *burst-matched* movements.

noted that the reduction in eye velocity is many times greater that the concurrent increase in head velocity. Two, consider that the number of spikes discharged by EBNs and IBNs is strongly linearly correlated with gaze amplitude with similar regression coefficients for HR and HU conditions (Cullen and Guitton 1997a,b; Ling et al. 1999). Thus instead of matching movements by burst profiles, we can pair them by gaze amplitude. We can then compare the peak eye-in-head velocity for gaze amplitude-matched movements (Fig. 15). It can be appreciated that for gaze shifts >25°, the reduction in peak eye velocity for HU movements is substantially more than the peak head velocity, which occurs well after the time of peak eye velocity; thus the head velocity at the time of peak eye velocity is even smaller. This is consistent with the results illustrated in Figs. 7*B* and 8*B,* which plots the difference in peak eye velocities for burst-matched movements. This should not be surprising because gaze amplitudes of burst matched movements are comparable (Fig. 6*E*). These two results downplay the importance of an exact match between HR and HU bursts. Our method does, however, provide insights into the time course of changes in eye velocity for a comparable oculomotor drive in HR and HU conditions and places limits on neural substrates that can implement the attenuation.

Neural mechanisms for attenuation in eye velocity

To explain why eye velocity decreases many times faster than the developing head movement during a HU gaze shift, Freedman (2001) proposed a model in which a head movement command lowers the gain of the brain stem burst generator that projects to the extraocular motoneurons (also see Kardamakis and Moschovakis 2009; Kardamakis et al. 2010). In other words, the firing rate of high-frequency BNs, the very same class of neurons pertinent to our study, is reduced during large amplitude gaze shifts, which in turn produces attenuation and/or dual peaks in the eye velocity waveform. According to the model, no attenuation in either BN activity or eye velocity is observed during HR saccades because there is no head movement command to lower the gain of the burst generator. Our results show that attenuation of BN activity cannot completely explain for the reduction in eye velocity because even when the BN activity is matched for HR and HU trials, the eye velocity is grossly attenuated in the presence of a head movement. We take these results to suggest that additional, perhaps alternative, mechanisms enforce the slower ocular saccade in HU condition.

One significant input to the abducens is of vestibular origin and arises from position-vestibular-pause (PVP) and eye-head (EH) neurons in the vestibular nuclei bilaterally. The activity of PVP cells conforms to the dogma that the VOR is at least partially suppressed during HU gaze shifts (Cullen et al. 2004; Guitton and Volle 1987; Laurutis and Robinson 1986; Lefèvre et al. 1992; Pélisson and Prablanc 1986; Pélisson et al. 1988; Tabak et al. 1996; Tomlinson 1990; Tomlinson and Bahra 1986). The VOR mechanism, however, requires that the reduction in eye velocity is not as large as the measured head velocity. Our attenuation index, in contrast, suggests that the decrease in eye velocity is many times greater than the instantaneous increase in head velocity. Thus it is unlikely that the PVPs can fully account for our observation.

The EH cells are thought to play a critical role in smooth pursuit eye movements (Cullen et al. 1993; Ghasia et al. 2008; Lisberger et al. 1994; McFarland and Fuchs 1992; Scudder and Fuchs 1992). Their role in mediating the VOR may be secondary to that of PVPs (Cullen and Roy 2004). It is clear that activity of EH neurons is modulated during both HR and HU gaze shifts (McCrea and Gdowski 2003; Roy and Cullen 2003). Furthermore, regression analyses performed on discharge rate of type II EH neurons shows that the eye velocity sensitivity is smaller for HU gaze shifts than for HR saccades (0.16 vs. 0.22) (Roy and Cullen 2003). These type II neurons make an excitatory connection to the contralateral abducens nucleus, suggesting that the eye velocity input is weaker in the HU condition. Thus the EH neurons are one likely source of enhanced attenuation in the eye velocity component of HU gaze shifts.

In addition to the putative EBNs and IBNs, abducens motoneurons also receive an oculomotor input from the neural integrator, which is thought to reside in the nucleus prepositus hypoglossi (Langer et al. 1986). While the textbook implication is that this region integrates the EBN phasic burst to produce a sustained tonic response, most neurons in this area exhibit both burst and tonic properties for HR saccades (Escudero et al. 1992; Hardy and Corvisier 1996; McFarland and Fuchs 1992). Such burst-tonic cells have not been studied during HU gaze shifts, however. We speculate that, like the type II EH neurons, the bust-tonic neurons also produce a weaker burst during a HU gaze shift, and both classes of neurons contribute to producing slower eye velocity. Additional neurophysiological studies on burst-tonic neurons are required to test the hypothesis.

ACKNOWLEDGMENTS

We thank Drs. Sean Anderson, Paul Dean, Carey Balaban, and Joe Furman for meaningful discussions, J. McFerron for programming maintenance, J. Buhrman for electronics assistance, and T. Wheeler for machine shop services. We are also grateful to the anonymous reviewers for insightful comments.

GRANTS

This work was supported by National Institutes of Health Grants R01-EY-015485, P30-DC-0025205, and P30-EY-008098.

DISCLOSURES

No conflicts of interest, financial or otherwise, are declared by the author(s).

REFERENCES

Bechara BP, Gandhi NJ. Properties of ocular counter-rotation during gaze shifts. *Soc Neurosci Abstr* 263.10, 2008.

Bock O. Load compensation in human goal-directed arm movements. *Behav Brain Res* 41: 167–177, 1990.

Bryant CL, Gandhi NJ. Real-time data acquisition and control system for the measurement of motor and neural data. *J Neurosci Methods* 142: 193–200, 2005.

Chen LL, Tehovnik EJ. Cortical control of eye and head movements: integration of movements and percepts. *Eur J Neurosci* 25: 1253–1264, 2007.

Choi WY, Guitton D. Firing patterns in superior colliculus of head-unrestrained monkey during normal and perturbed gaze saccades reveal short-latency feedback and a sluggish rostral shift in activity. *J Neurosci* 29: 7166–7180, 2009.

Cohen B, Henn V. Unit activity in the pontine reticular formation associated with eye movements. *Brain Res* 46: 403–410, 1972.

Cullen KE, Chen-Huang C, McCrea RA. Firing behavior of brain stem neurons during voluntary cancellation of the horizontal vestibuloocular reflex. II. Eye movement related neurons. *J Neurophysiol* 70: 844–856, 1993.

Cullen KE, Guitton D. Analysis of primate IBN spike trains using system identification techniques. I. Relationship to eye movement dynamics during head-fixed saccades. *J Neurophysiol* 78: 3259–3282, 1997a.

Cullen KE, Guitton D. Analysis of primate IBN spike trains using system identification techniques. II. Relationship to gaze, eye, and head movement dynamics during head-free gaze shifts. *J Neurophysiol* 78: 3283–3306, 1997b.

Cullen KE, Huterer M, Braidwood DA, Sylvestre PA. Time course of vestibuloocular reflex suppression during gaze shifts. *J Neurophysiol* 92: 3408–3422, 2004.

Cullen KE, Roy JE. Signal processing in the vestibular system during active versus passive head movements. *J Neurophysiol* 91: 1919–1933, 2004.

Escudero M, de la Cruz RR, Delgado-Garcia JM. A physiological study of vestibular and prepositus hypoglossi neurones projecting to the abducens nucleus in the alert cat. *J Physiol* 458: 539–560, 1992.

Evinger C, Manning KA, Pellegrini JJ, Basso MA, Powers AS, Sibony PA. Not looking while leaping: the linkage of blinking and saccadic gaze shifts. *Exp Brain Res* 100: 337–344, 1994.

Freedman EG. Interactions between eye and head control signals can account for movement kinematics. *Biol Cybern* 84: 453–462, 2001.

Freedman EG, Sparks DL. Eye-head coordination during head-unrestrained gaze shifts in rhesus monkeys. *J Neurophysiol* 77: 2328–2348, 1997.

Freedman EG, Sparks DL. Coordination of the eyes and head: movement kinematics. *Exp Brain Res* 131: 22–32, 2000.

Galiana HL, Guitton D. Central organization and modeling of eye-head coordination during orienting gaze shifts. *Ann NY Acad Sci* 656: 452–471, 1992.

Gandhi NJ. Consequence of blinks on interactions between the eye and head components of gaze shifts. *Soc Neurosci Abstr* 178.2, 2007.

Gandhi NJ, Bonadonna DK. Temporal interactions of air-puff evoked blinks and saccadic eye movements: insights into motor preparation. *J Neurophysiol* 93: 1718–1729, 2005.

Gandhi NJ, Sparks DL. Experimental control of eye and head positions prior to head-unrestrained gaze shifts in monkey. *Vision Res* 41: 3243–3254, 2001.

Ghasia FF, Meng H, Angelaki DE. Neural correlates of forward and inverse models for eye movements: evidence from three-dimensional kinematics. *J Neurosci* 28: 5082–5087, 2008.

Grantyn A, Ong-Meang Jacques V, Berthoz A. Reticulo-spinal neurons participating in the control of synergic eye and head movements during orienting in the cat. II. Morphological properties as revealed by intra-axonal injections of horseradish peroxidase. *Exp Brain Res* 66: 355–377, 1987.

Guitton D, Volle M. Gaze control in humans: eye-head coordination during orienting movements to targets within and beyond the oculomotor range. *J Neurophysiol* 58: 427–459, 1987.

Hardy O, Corvisier J. Firing properties of preposito-collicular neurones related to horizontal eye movements in the alert cat. *Exp Brain Res* 110: 413–424, 1996.

Hepp K, Henn V. Spatio-temporal recoding of rapid eye movement signals in the monkey paramedian pontine reticular formation (PPRF). *Exp Brain Res* 52: 105–120, 1983.

Hu X, Jiang H, Gu C, Li C, Sparks DL. Reliability of oculomotor command signals carried by individual neurons. *Proc Natl Acad Sci USA* 104: 8137–8142, 2007.

Kaneko CRS. Saccade-related, long-lead burst neurons in the monkey rostral pons. *J Neurophysiol* 95: 979–994, 2006.

Kaneko CR, Evinger C, Fuchs AF. Role of cat pontine burst neurons in generation of saccadic eye movements. *J Neurophysiol* 46: 387–408, 1981.

Kardamakis AA, Grantyn A and Moschovakis AK. Neural network simulations of the primate oculomotor system. V. Eye-head gaze shifts. *Biol Cybern* 2010.

Kardamakis AA, Moschovakis AK. Optimal control of gaze shifts. *J Neurosci* 29: 7723–7730, 2009.

Keller EL. Participation of medial pontine reticular formation in eye movement generation in monkey. *J Neurophysiol* 37: 316–332, 1974.

Keller EL, McPeek RM, Salz T. Evidence against direct connections to PPRF EBNs from SC in the monkey. *J Neurophysiol* 84: 1303–1313, 2000.

Langer T, Kaneko CR, Scudder CA, Fuchs AF. Afferents to the abducens nucleus in the monkey and cat. *J Comp Neurol* 245: 379–400, 1986.

Laurutis VP, Robinson DA. The vestibulo-ocular reflex during human saccadic eye movements. *J Physiol* 373: 209–233, 1986.

Lefèvre P, Bottemanne I, Roucoux A. Experimental study and modeling of vestibulo-ocular reflex modulation during large shifts of gaze in humans. *Exp Brain Res* 91: 496–508, 1992.

Lehnen N, Büttner U, Glasauer S. Vestibular guidance of active head movements. *Exp Brain Res* 194: 495–503, 2009.

Ling L, Fuchs AF, Phillips JO, Freedman EG. Apparent dissociation between saccadic eye movements and the firing patterns of premotor neurons and motoneurons. *J Neurophysiol* 82: 2808–2811, 1999.

Lisberger SG, Pavelko TA, Broussard DM. Neural basis for motor learning in the vestibuloocular reflex of primates. I. Changes in the responses of brain stem neurons. *J Neurophysiol* 72: 928–953, 1994.

Luschei ES, Fuchs AF. Activity of brain stem neurons during eye movements of alert monkeys. *J Neurophysiol* 35: 445–461, 1972.

McCrea RA, Gdowski GT. Firing behaviour of squirrel monkey eye movement-related vestibular nucleus neurons during gaze saccades. *J Physiol* 546: 207–224, 2003.

McFarland JL, Fuchs AF. Discharge patterns in nucleus prepositus hypoglossi and adjacent medial vestibular nucleus during horizontal eye movement in behaving macaques. *J Neurophysiol* 68: 319–332, 1992.

Pélisson D, Prablanc C. Vestibulo-ocular reflex (VOR) induced by passive head rotation and goal-directed saccadic eye movements do not simply add in man. *Brain Res* 380: 397–400, 1986.

Pélisson D, Prablanc C, Urquizar C. Vestibuloocular reflex inhibition and gaze saccade control characteristics during eye-head orientation in humans. *J Neurophysiol* 59: 997–1013, 1988.

Quaia C, Optican LM. Model with distributed vectorial premotor bursters accounts for the component stretching of oblique saccades. *J Neurophysiol* 78: 1120–1134, 1997.

Rambold H, Sprenger A, Helmchen C. Effects of voluntary blinks on saccades, vergence eye movements, and saccade-vergence interactions in humans. *J Neurophysiol* 88: 1220–1233, 2002.

Robinson DA. Oculomotor control signals. In: *Basic Mechanisms of Ocular Motility and Their Clinical Implications*, edited by Bach-y-Rita P, Lennerstrand G. Oxford: Pergamon, 1975, p. 337–374.

Rottach KG, Das VE, Wohlgemuth W, Zivotofsky AZ, Leigh RJ. Properties of horizontal saccades accompanied by blinks. *J Neurophysiol* 79: 2895–2902, 1998.

Roy JE, Cullen KE. Brain stem pursuit pathways: dissociating visual, vestibular, and proprioceptive inputs during combined eye-head gaze tracking. *J Neurophysiol* 90: 271–290, 2003.

Scudder CA, Fuchs AF. Physiological and behavioral identification of vestibular nucleus neurons mediating the horizontal vestibuloocular reflex in trained rhesus monkeys. *J Neurophysiol* 68: 244–264, 1992.

Scudder CA, Fuchs AF, Langer TP. Characteristics and functional identification of saccadic inhibitory burst neurons in the alert monkey. *J Neurophysiol* 59: 1430–1454, 1988.

Scudder CA, Kaneko CS, Fuchs AF. The brainstem burst generator for saccadic eye movements: a modern synthesis. *Exp Brain Res* 142: 439–462, 2002.

Sparks DL. Conceptual issues related to the role of the superior colliculus in the control of gaze. *Curr Opin Neurobiol* 9: 698–707, 1999.

Sparks DL, Gandhi NJ. Single cell signals: an oculomotor perspective. *Prog Brain Res* 142: 35–53, 2003.

Strassman A, Highstein SM, McCrea RA. Anatomy and physiology of saccadic burst neurons in the alert squirrel monkey. I. Excitatory burst neurons. *J Comp Neurol* 249: 337–357, 1986a.

Strassman A, Highstein SM, McCrea RA. Anatomy and physiology of saccadic burst neurons in the alert squirrel monkey. II. Inhibitory burst neurons. *J Comp Neurol* 249: 358–380, 1986b.

Sylvestre PA, Cullen KE. Premotor correlates of integrated feedback control for eye-head gaze shifts. *J Neurosci* 26: 4922–4929, 2006.

Tabak S, Smeets JB, Collewijn H. Modulation of the human vestibuloocular reflex during saccades: probing by high-frequency oscillation and torque pulses of the head. *J Neurophysiol* 76: 3249–3263, 1996.

Tomlinson RD. Combined eye-head gaze shifts in the primate. III. Contributions to the accuracy of gaze saccades. *J Neurophysiol* 64: 1873–1891, 1990.

Tomlinson RD, Bahra PS. Combined eye-head gaze shifts in the primate. II. Interactions between saccades and the vestibuloocular reflex. *J Neurophysiol* 56: 1558–1570, 1986.

Van Gisbergen JA, Robinson DA, Gielen S. A quantitative analysis of generation of saccadic eye movements by burst neurons. *J Neurophysiol* 45: 417–442, 1981.

Van Horn MR, Sylvestre PA, Cullen KE. The brain stem saccadic burst generator encodes gaze in three-dimensional space. *J Neurophysiol* 99: 2602–2616, 2008.

Walton MMG, Bechara BP, Gandhi NJ. Role of the primate superior colliculus in the control of head movements. *J Neurophysiol* 98: 2022–2037, 2007.

Walton MMG, Freedman EG. Discharge characteristics of pontine reticular formation neurons in head unrestrained primates. *Soc Neurosci Abstr* 851.4, 2009.

Yoshida K, McCrea R, Berthoz A, Vidal PP. Morphological and physiological characteristics of inhibitory burst neurons controlling horizontal rapid eye movements in the alert cat. *J Neurophysiol* 48: 761–784, 1982.

Zhou W, King WM. Premotor commands encode monocular eye movements. *Nature* 393: 692–695, 1998.